Riemann surfaces of complex classical trajectories and tunnelling splitting in one-dimensional systems

Hiromitsu Harada

Department of Physics

Tokyo Metropolitan University

A thesis submitted in partial fulfillment of

the requirements for the degree of

Doctor of Philosophy in Science

to

Tokyo Metropolitan University

2018

Contents

Abstract

Tunnelling splitting in integrable systems is studied in the semiclassical regime. The semiclassical formula of the tunnelling splitting requires certain complex trajectories as input for it. We mainly discuss how the complex trajectories with different topologies can be obtained. It has been a standard strategy, as is the case of the so called the instanton path, to explore complex trajectories in the time plane. However it would not be practically possible or feasible to enumerate all topologically distinct complex paths required by the semiclassical analysis of tunnelling splittings. This point will be closely examined by providing analytical solutions for some simple Hamiltonian systems and then showing that infinitely many singularities appear in the complex time plane. Here we claim that, instead of considering the complex trajectories in the time plane, one should analyse complex trajectories in the configuration space. In order to illustrate this, we here examine the Hamiltonian expressed as polynomial functions. As a result of limiting ourselves to such a class of systems, it turns out that the Riemann surface of complex trajectory is homeomorphic to a compact space. The fundamental group for the corresponding Riemann surface provides complete information of the topology of complex paths, and enables us to enumerate all possible candidates contributing to the semiclassical sum formula for tunnelling splittings. This naturally leads to action relations among classically disjoint regions, revealing entirely non-local nature of the quantization condition. The importance of the treatment of the Stokes phenomenon is also discussed in the case of Hamiltonians in the normal form.

Chapter 1

Introduction

In this thesis, we will study the tunnelling phenomenon in 1-dimensional systems. This is motivated by recent studies on quantum tunnelling in multi-dimensional systems, especially non-integrable systems [1–7]. Many attempts have so far been made in order to understand multi-dimensional tunnelling. However, not only conceptually but also technically there still exist many issues, which remain unsolved and wait for our further investigations. Among them, some originate not necessarily from the fact that systems under consideration are multi-dimensional or non-integrable, but that important tools we use for analyses has not satisfactorily been developed even for 1-dimensional situations. As explained below, the semiclassical theory especially for 1-dimensional quantum tunnelling is not ripe enough to tackle the problems we are facing.

In classical mechanics, 1-dimensional Hamiltonian systems are integrable and exhibit regular motions such as ballistic or periodic motion [8–10]. On the other hand, multi-dimensional Hamiltonian systems are in general non-integrable and exhibit not only regular motion but also chaotic motion. The non-integrable systems lack analytical solutions to the equations of motion, therefore we usually discuss the dynamics by observing the phase space of the system numerically. The phase space in multi-dimensional systems shows chaotic regions and nonlinear resonances, which are characteristic dynamical structures of non-integrable systems.

Tunnelling is a typical quantum phenomenon by which a particle penetrates into classically forbidden regions. For instance, in the 1-dimensional double-well system, two wells are separated by a potential barrier. Classical particles with energies below the top of the potential barrier would

oscillate in each well, without being able to move beyond the potential barrier. In quantum mechanics, however, a particle can penetrate into the barrier and move beyond it. This penetration is called barrier tunnelling. In multi-dimensional systems, even without potential barriers, a particle can be confined in limited regions. This is because orbits in each constant energy surface are divided into (infinitely many) regions in each of which the orbits are confined. The orbits in phase space of multi-dimensional systems could therefore be separated *dynamically*. Alternatively stated, each orbit plays a role of barrier to other orbits, like potential barriers in 1-dimensional systems, so it would be reasonable, analogous to the potential barrier tunnelling, to consider tunnelling penetration through dynamically formed barriers. This type of tunnelling is called *dynamical tunnelling* in literatures [11–13].

Tunnelling splitting is a well-known manifestation of quantum tunnelling: tunnelling splitting is given as a difference between quasi-degenerate eigenenergies associated with symmetric and anti-symmetric combinations of the eigenfunctions localized in each well. It is typically discussed in the 1-dimensional symmetric double-well potential system [14–18]. Here we will focus on tunnelling splitting and try to relate it to the underlying classical mechanics since our ultimate goal is to clarify how integrability of classical mechanics manifests itself in quantum tunnelling.

In the past two decades, it has been reported that quantum tunnelling is affected by chaos and nonlinear resonances in the classical phase space. The role of classical chaos in quantum tunnelling has been observed in quantum wave packet dynamics [1], as well as in tunnelling splitting [2–5]. In multi-dimensional systems, it has been shown that the classical chaos and nonlinear resonances in the classical phase space drastically enhance the tunnelling splitting, compared to the case for 1-dimensional systems; these phenomena are called chaos-assisted tunnelling (CAT) [5] and resonance-assisted tunnelling (RAT) [6, 7], respectively. However, there is no evidence showing that the enhancement could not appear in 1-dimensional, integrable systems. If such enhancement took place even in 1-dimensional systems, the concept of RAT and CAT should be reconsidered. One might of course expect that the nature of tunnelling is essentially different between integrable and non-integrable systems and the enhancement is the nature owned only by non-integrable systems. However, no one has yet confirmed this explicitly, and we need more convincing explanations why we can say so.

Semiclassical theory has been used and is known to be an efficient tool to understand the relation between classical and quantum mechanics. Concerning tunnelling splittings, a formula for the double-well potential system was derived by taking the trace of propagator in the form of the Feynman path integral [19]. In particular, the idea of *instanton* was proposed in [20] as an input of the semiclassical formula for tunnelling splittings and was first applied to gauge field theories to describe tunnelling between degenerate vacua [19, 21]. Later complexifying time has become a widely used technique and now there are numerous applications [22–34].

Even under such circumstances, the semiclassical formulation for tunnelling splittings beyond the double-well potential situation is quite limited. To the best of our knowledge, the work by Le Deunff and Mouchet [35] first derived a semiclassical formula which could be applied to the triple-well potential system. Needless to say, it is far beyond our reach to develop similar arguments made there and to obtain formulas applicable to multi-dimensional or non-integrable systems. Hence we will extensively employ the formula derived in Ref. [35] in our subsequent study since it is the only formula that can be applied to tunnelling splitting in the situation beyond the double-well potential system.

There are two tasks that must be made to establish a semiclassical analysis of tunnelling splitting. The first step is to enumerate all possible complex trajectories that satisfy the boundary conditions required by the semiclassical formula. The second step is to deal with the so-called Stokes phenomenon, which generally occurs when one applies the saddle point approximation to integrals. Due to the Stokes phenomenon, it is known that not all of the complex trajectories contribute to the saddle point evaluation.

In the symmetric triple-well system, the tunnelling splitting as a function of $1/\hbar$ exhibits exponential decay accompanied with a sequence of spikes. Such enhancements in such a situation are known as so called resonant tunnelling [35, 36]. The authors in [35] succeeded in reproducing these spikes based on a semiclassical analysis using classical trajectories in the complex time plane. However, since they searched complex trajectories only numerically, we need more convincing evidence why it works even though there exist (infinitely) many other complex trajectories [35]. The paper's argument would need to be reconsidered if there exists at least one complex path with a

dominant contribution to the semiclassical formula other than those studied in [35].

In this thesis, we mainly discuss the first step, i.e., finding a systematic way to enumerate all complex trajectories. One of main results of this thesis is that considering trajectories in the complex time plane is not a right strategy for semiclassical analysis of tunnelling splitting, even though there have been a lot of works along this line. The reason for this is that, as will be shown, the solution of the equations of motion as a function of time has infinitely many singularities. As a result, there are infinitely many topologically distinct complex trajectories. This fact makes it impossible to enumerate all complex trajectories in general. We suggest that one should examine the complex trajectories on the configuration space instead of the complex time plane. To illustrate this we here take the Hamiltonian which is expressed as a polynomial function of momentum and position. Then any local classical quantities are algebraic functions of dynamical variables. This makes the Riemann surface simple, allowing all complex trajectories to be enumerated. Our method for enumerating these trajectories can be applied not only to the triple-well potential system but also to multi-well potential systems. This result will help to establish semiclassical analysis for integrable systems.

This thesis is organized as follows. In chapter 2, we briefly review the enhancement of the tunnelling splitting in the light of RAT, as well as the semiclassical argument of the tunnelling splitting in a couple of 1-dimensional systems with trajectories on the complex-time plane. We show that infinitely many singularities on the time plane hinder our enumeration of complex trajectories. In chapter 3, we discuss the semiclassical formula for the tunnelling splitting and reconsider complex-trajectory enumeration. We explain our strategy for enumerating topologically distinct complex trajectories. The key idea is to examine the complex trajectories on the configuration space instead of the complex time plane. By doing so, the fundamental group of the Riemann surfaces for the corresponding function will make it possible to obtain a complete list of complex trajectories. In chapter 4, we apply our method introduced in chapter 3 to 1-dimensional double- and triple-well potential systems. For the second step, we handle the Stokes phenomenon in a heuristic manner, i.e., eliminating exponentially exploding unphysical solutions. After dealing with the Stokes phenomenon, we evaluate the tunnelling splitting by using specific trajectories which have the smallest imaginary action, because such trajectories have the most dominant contribution to the semiclas-

sical tunnelling splitting formula. The results obtained here are the same as already known results in [35]. As a byproduct, we obtain non-trivial global relations among action integrals, leading to a simultaneous quantization condition for distinct potential wells. We further investigate a normal form of the Hamiltonian system. In that case, we also obtain a complete list of complex trajectories but we show that our heuristic manner of handling the Stokes phenomenon does not work. In chapter 5, we summarise this thesis and discuss future works.

Chapter 2

Tunnelling splitting and semiclassical analysis

2.1 Resonance-assisted tunnelling

In the 1-dimensional symmetric double-well potential system, quantum tunnelling manifests as exponentially small energy splittings, caused by the coupling between odd and even eigenstates forming quasi-degenerated doublets. It is known that the splitting width decays exponentially as a function of $1/\hbar$ and the way of decay is always monotonic. However, more than 1-dimensional systems, the nature of quantum tunnelling drastically changes, reflecting the fact that the system is in general non-integrable and chaos appears in the corresponding classical dynamics [13]. In fact, the role of chaos in quantum tunnelling was first investigated in wavepacket dynamics [1], and in tunnelling splittings as well [2–5]. These works have focused mainly on the role of chaos, and the tunnelling effect associated with classical chaos was called "chaos-assisted tunnelling" in [5]. Later the effect of nonlinear resonances to quantum tunnelling has also been explored [6, 7]. The emergence of nonlinear resonances is also a generic phenomenon in non-integrable systems, so it would be fairly reasonable to study the role of nonlinear resonances in quantum tunnelling. The authors of Ref. [6, 7] have put a name "resonance-assisted tunnelling" to a phenomenon which could be invoked by nonlinear resonances appearing in the classical phase space. In both situations, chaos-assisted and resonance-assisted tunnelling, it has been claimed that the tunnelling probability

is drastically enhanced as compared to that observed in 1-dimensional systems.

In this section, we will explain how the enhancement of tunnelling in the nearly-integrable system is observed. Let us consider the standard map system as an example in order to discuss the enhancement of tunnelling splitting. The standard map is known to have generic features of nearly-integrable systems, in which chaos and nonlinear resonances appear in the phase space [37]. Since we here consider the tunnelling splitting, we will use the version in which the original form of the standard map is modified as [1]

$$F : \begin{cases} p_{n+1} = & p_n + 2k\sin(2q_n) \\ q_{n+1} = & q_n + p_{n+1}\tau. \end{cases} \tag{2.1}$$

The map system describes the motion of a particle with discrete time, so the trajectory of a particle is described by the discrete time evolution: $(q_n, p_n) \to (q_{n+1}, p_{n+1})$, where q_n is the position and p_n the momentum of the particle at each time step n. The map is derived from the equations of motion for the so-called kicked Hamiltonian:

$$H(p, q, t) = \frac{p^2}{2} + k\cos(2q)\sum_n \delta(n\tau - t), \tag{2.2}$$

and q_n, p_n are obtained by the integration of the Hamiltonian equations of motion over the period τ. This map could also be regarded as discretization of the Hamiltonian equations of motion for the 1-dimensional pendulum

$$H = \frac{p^2}{2} + k\cos(2q), \tag{2.3}$$

and τ shows the discretization interval. Typical examples of phase space portraits are presented in figure 2.1.

For $\tau = 1$, the system is nearly-integrable, the most dominant nonlinear resonances are located at $(q, p) = (\pi/2, 0)$ and $(3\pi/2, 0)$, and there appear chaotic motions around an unstable fixed point at $(q, p) = (\pi, 0)$. However, chaotic regions do not spread over the entire phase space but are

[1] This model was used in [38] to study tunnelling splitting in the nearly-integrable system.

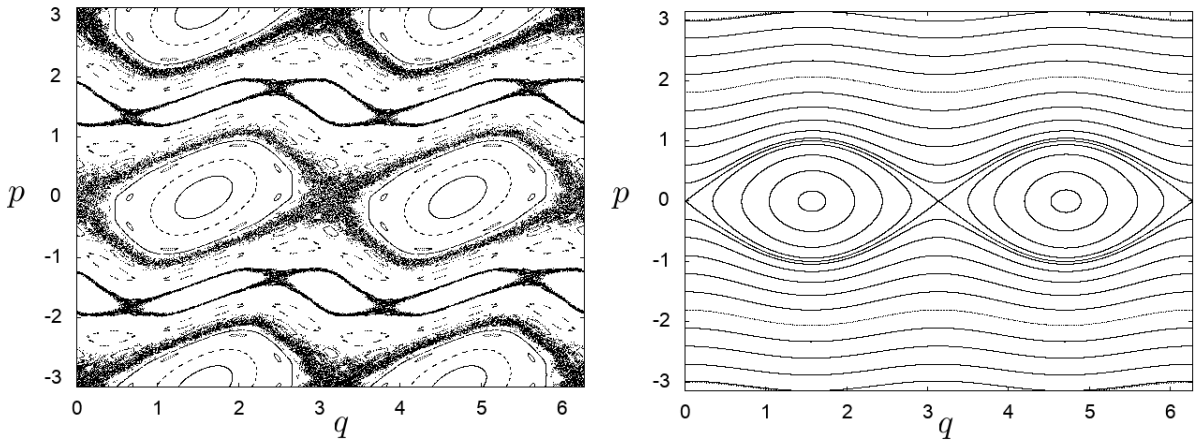

Figure 2.1: The phase space of the standard map with $k = 0.25$. (Left) The case of $\tau = 1$. Both chaotic orbits and nonlinear resonances (small circles around wells) are visible. (Right) The case of $\tau \sim 0$. Regular orbits dominate the phase space, which is very close to the phase space for the 1-dimensional pendulum.

localized only in the vicinity of an unstable fixed point. The term "nearly" comes from such an aspect of phase space. Most of signatures of the integrable limit $\tau \sim 0$ still remain, and the phase space is covered by regular orbits, shown as continuous curves, and is very close to the phase space of the pendulum Hamiltonian.

The corresponding quantum map can be formulated by introducing the unitary operator given as

$$\hat{U}(\tau) = \exp\left(-\frac{\mathrm{i}}{\hbar}\frac{\hat{p}^2}{2}\tau\right)\exp\left(-\frac{\mathrm{i}}{\hbar}k\cos(2\hat{q})\tau\right). \tag{2.4}$$

The associated eigenvalue equation is expressed as

$$\hat{U}(\tau)|\psi_n\rangle = \exp\left(-\frac{\mathrm{i}}{\hbar}\epsilon_n\tau\right)|\psi_n\rangle, \tag{2.5}$$

where ϵ_n is called quasi-eigenenergy. Here tunnelling splitting of quasi-eigenvalues appears between odd and even quasi-eigenstates, which are both localized on invariant curves surrounding the most dominant nonlinear resonance but have different parity, analogous to the symmetric double-well potential system as explained above. The splitting is therefore defined as $\Delta E := \epsilon_n^- - \epsilon_n^+$, where $\epsilon_n^\pm$ are quasi-eigenvalues associated with even and odd parity, respectively. The ΔE numer-

ically calculated in this way is shown in figure 2.2.

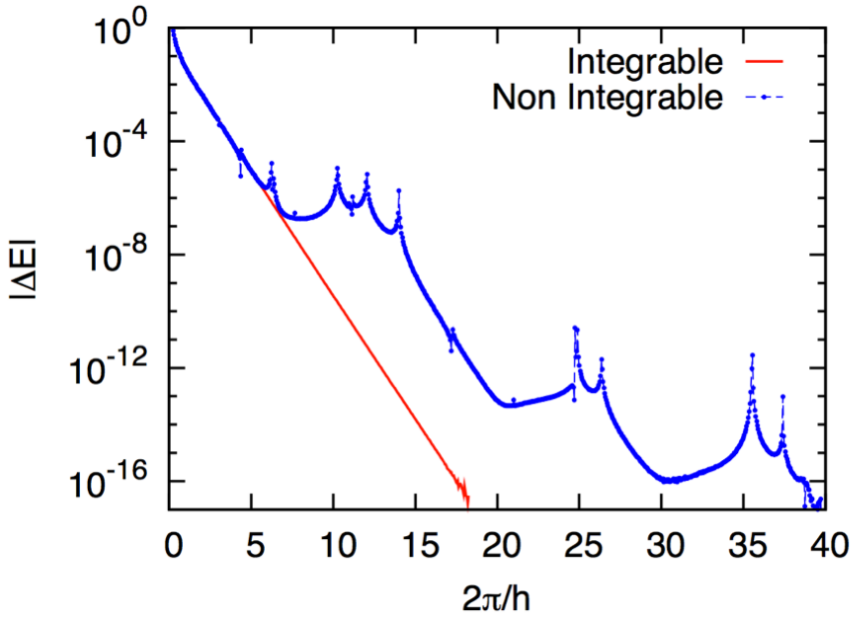

Figure 2.2: The tunnelling splitting ΔE as a function of $2\pi/\hbar$ for the quantum standard map system. The blue line shows the case of $\tau = 1$, the red line the case of $\tau \sim 0$.

As shown in figure 2.2, the tunnelling splitting ΔE for the case $\tau \sim 0$ shows a simple exponentially decaying behaviour whereas that for $\tau = 1$ exhibits a staircase like structure accompanied by spikes.

The plot ΔE vs $1/\hbar$ for the non-integrable map was first made in [4] and the enhancement shown here was recognised in [39], and later closely examined in [6,7]. In particular, the authors of Ref. [6, 7] attributed such enhancement to the existence of nonlinear resonances in classical phase space. To explain it, they developed a hybrid scheme based on quantum perturbation analysis whose ingredients are taken from the classical phase space. It was reported that, after several technical improvements, such a scheme could successfully reproduce analogous quantities, not exactly tunnelling splittings, associated with tunnelling [40]. Since their approach is based on classical nonlinear resonances, they call such a tunnelling mechanism "resonance-assisted tunnelling".

On the other hand, recent studies [41, 42] are revealing that the role of nonlinear resonances is rather restricted, just creating spikes in ΔE vs $1/\hbar$ plot. This was confirmed by applying selective absorbers composed of well tuned basis functions in order to eliminate the coupling to the states

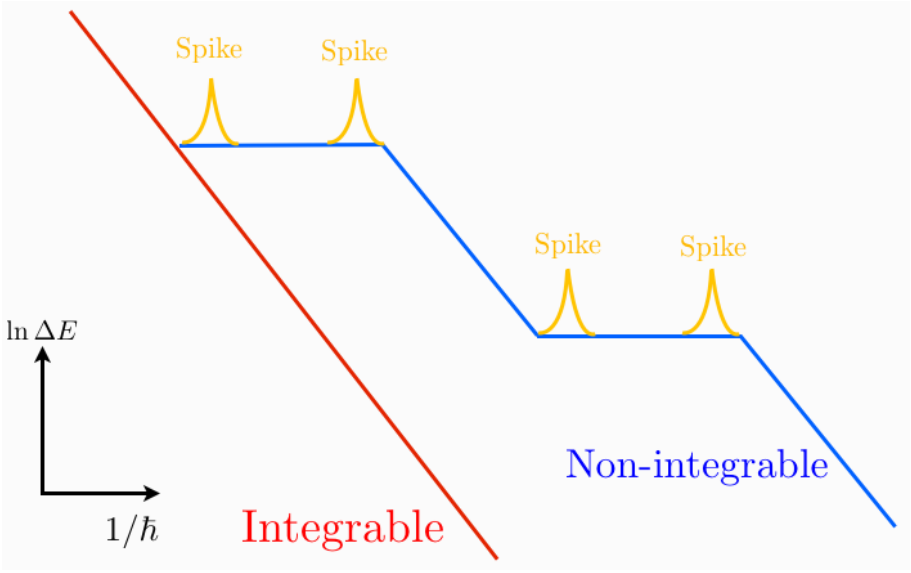

Figure 2.3: The figure illustrates the difference of signatures observed in $\tau \sim 0$ and $\tau = 1$. In Ref. [41], the latter curve is interpreted as the one composed of the backbone staircase (blue) and spikes (yellow) on it.

responsible for creating spikes. They have observed that even though spikes disappear under such operation the staircase structure survives, meaning that the staircase structure, the most important signature in tunnelling splitting in non-integrable systems, could not be attributed to the states associated with classical nonlinear resonances. The origin of the staircase structure was further examined in details in Ref. [41].

In order to establish that classical nonlinear resonances or even chaos do not provide a source creating the staircase behaviour in ΔE vs $1/\hbar$ plot, it would be necessary to see this issue also from the integrable side, because there is no evidence confirming that the staircase cannot appear in integrable systems. If it is true that the staircase structure cannot appear in integrable systems, the latter perspective turns out to acquire another supports. On the other hand, if the staircase structure appears even in the integrable limit, the concept of resonance-assisted and chaos-assisted tunnelling should be reconsidered.

2.2 Double-well potential and instanton

In this section, we will briefly review tunnelling splittings in the double-well potential system and introduce the so-called instanton. Let us consider a 1-dimensional symmetric double-well potential system,

$$H(p,q) = \frac{p^2}{2} + V(q), \tag{2.6}$$

$$V(q) = (q^2 - a^2)^2. \tag{2.7}$$

The potential function $V(q)$ has two minima at $q = \pm a$. The portrait of the phase space is shown in figure 2.4.

The time-independent Schrödinger equation is

$$\hat{H}|\phi_n^{\pm}\rangle = E_n^{\pm}|\phi_n^{\pm}\rangle, \tag{2.8}$$

where $E_n^{\pm}$ and $\phi_n^{\pm}$ are the eigenvalues and the corresponding eigenfunctions, respectively. The $\pm$ signs denote the parity of eigenfuncions with respect to the q direction.

The state $|L\rangle := |\phi_0^-\rangle + |\phi_0^+\rangle$ localizes at the left-well, and the state $|R\rangle := |\phi_0^-\rangle - |\phi_0^+\rangle$ localizes at the right-well. The time evolution of the state $|L\rangle$ driven by the time evolution operator $\hat{U}(T) = e^{-\mathrm{i}\hat{H}T/\hbar}$ is expressed as

$$\begin{aligned}
\hat{U}(T)|L\rangle &= e^{-\mathrm{i}E_0^+T/\hbar}|\phi_0^+\rangle + e^{-\mathrm{i}E_0^-T/\hbar}|\phi_0^-\rangle \\
&= e^{-\mathrm{i}E_0^+T/\hbar}(|\phi_0^+\rangle + e^{-\mathrm{i}(E_0^- - E_0^+)T/\hbar}|\phi_0^-\rangle) \\
&= e^{-\mathrm{i}E_0^+T/\hbar}(|\phi_0^+\rangle + e^{-\mathrm{i}\Delta ET/\hbar}|\phi_0^-\rangle),
\end{aligned} \tag{2.9}$$

where $\Delta E := E_0^- - E_0^+$. Within the time interval $T = \pi\hbar/\Delta E$, the wavepacket $|L\rangle$ moves to $|R\rangle$. It is obvious that the state $|L\rangle$ oscillates between two wells with the period $T = 2\pi\hbar/\Delta E$. This oscillation is called tunnelling oscillation and the associated energy difference ΔE is called tunnelling splitting (For instance, see [17].).

As is well known [14], the tunnelling splitting ΔE is semiclassically evaluated as

$$\Delta E \sim A e^{-S_{\rm cl}/\hbar}, \tag{2.10}$$

where $S_{\rm cl}$ is the classical action integral:

$$S_{\rm cl} = \int_{-a}^{a} \sqrt{2(E - V(q))} dq, \tag{2.11}$$

and A is a prefactor. Integration is made along classical paths which connect the bottoms of the wells. When rotating the time direction as $t \to -{\rm i}\tau$, which is called the Wick rotation, one obtains a solution for classical equations of motion as

$$q(\tau) = a \tanh(a\sqrt{2}(\tau - \tau_0)), \tag{2.12}$$

where τ_0 denotes a critical time at which the path goes over the potential barrier. This complex path is called the instanton [18, 21]. The action of the instanton gives us a semiclassical evaluation of tunnelling splitting in the formula (2.10).

In general, complex paths run in 2-dimensional complex phase space, or 4-dimensional real space $({\rm Re}\, q, {\rm Re}\, p, {\rm Im}\, q, {\rm Im}\, p)$. However the instanton derived above is confined onto the $({\rm Re}\, q, {\rm Im}\, p)$ plane, so the intanton could be visualized by projecting onto $({\rm Re}\ q, {\rm Re}\ p, {\rm Im}\ p)$ space, which is shown in figure 2.4.

2.3 Triple-well potential and complex path

In this section, we review a semiclassical analysis of tunnelling splitting in the symmetric triple-well system studied in [35]. The system studied in [35] is as follows,

$$H(p, q) = \frac{p^2}{2} + V(q), \tag{2.13}$$

$$V(q) = (q^2 - a^2)^2 (q^2 - b^2). \tag{2.14}$$

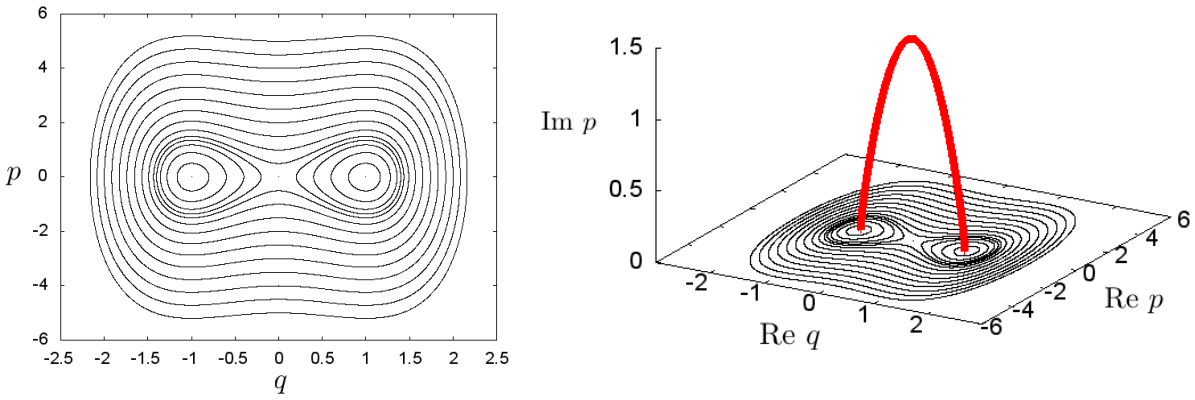

Figure 2.4: (Left) The phase space of the double-well model (2.7) with $a = 1$. (Right) A projection of instanton onto $(\mathrm{Re}\ q, \mathrm{Re}\ p, \mathrm{Im}\ p)$ space.

The potential portrait is depicted in figure 2.5. The potential has two symmetrically located wells at $q = \pm a$ and a central well at $q = 0$. The classical phase space is shown at the left side of figure 2.7.

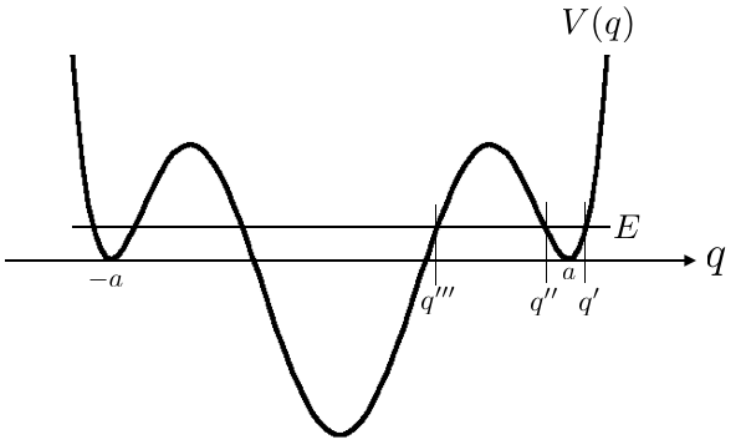

Figure 2.5: The triple-well potential.

The tunnelling splitting $\Delta E_n := E_n^- - E_n^+$ is defined as well as the double-well case, where E_n^- and E_n^+ are eigenvalues for the odd and even parity states with respect to the q direction. We show in figure 2.6 a typical behaviour of tunnelling splittings as a function of $1/\hbar$, and observe that a sequence of spikes appears in the plot. The origin of the spikes has been closely argued and

it was attributed to the so-called resonant tunnelling effect [35, 36].

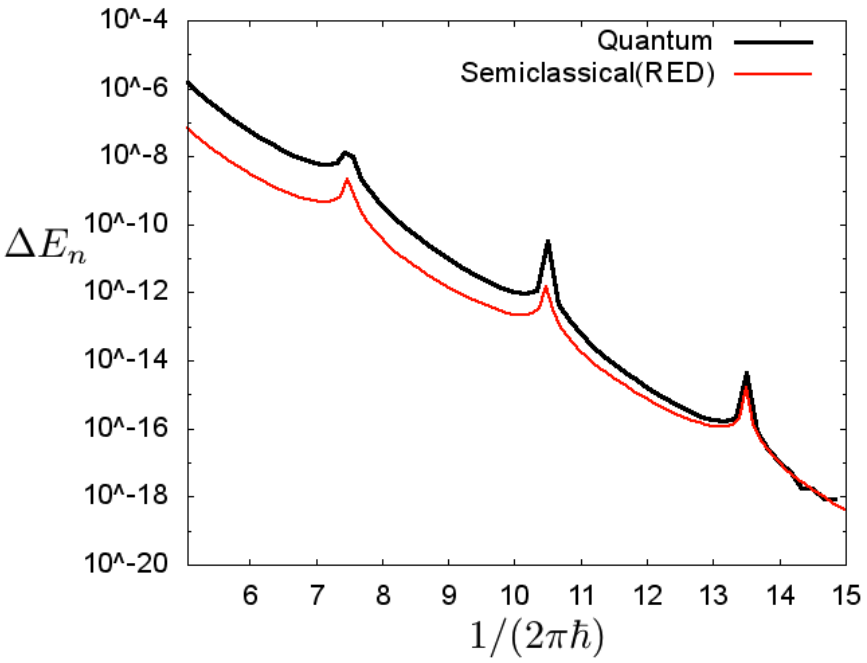

Figure 2.6: Tunnelling splittings ΔE obtained by direct diagonalization (black) and by using the semiclassical formula (red).

If the height of the central well is smaller than that of both wells, tunnelling splittings in the triple-well potential appear in the exited states, while the formula (2.10) is applicable only to the tunnelling splitting between the ground and first exited state. In Ref. [35], a semiclassical formula for tunnelling splittings of exited states has been derived. We briefly show the sketch of their derivation in Appendix B and section 3.1. Within a rather heuristic argument, the authors of Ref. [35] has picked up certain specific complex trajectories to calculate the tunnelling splitting for the triple-well system. The resulting semiclassical formula taking into account such complex trajectories turns out to take the form as

$$\Delta E_n \sim \frac{\hbar}{T_r} e^{-2S_c/\hbar} \sum_{w_r, w_m} (w_r + 1) e^{\mathrm{i}w_r(S_r/\hbar - \pi) + \mathrm{i}w_m(S_m/\hbar - \pi)}, \tag{2.15}$$

where S_r and S_m are the actions of the real periodic orbits at the energy $E \sim E_n^{\pm}$ located in right

and centre well, respectively:

$$S_r := 2\int_{q''}^{q'} \sqrt{2(E-V(q))}dq, \tag{2.16}$$

$$S_m := 4\int_{0}^{q'''} \sqrt{2(E-V(q))}dq, \tag{2.17}$$

and w_r and w_m represent the winding numbers. T_r denotes the period of the right well [2]. S_c is the actions of "instantons":

$$S_c := \int_{q'''}^{q''} \sqrt{2(E-V(q))}dq. \tag{2.18}$$

$$\tag{2.19}$$

The complex path taken in Ref. [35] is shown in the right panel of figure 2.7. The path is a combination of the real periodic orbits running in the both wells and the "instanton" bridging the wells. The final semiclassical formula could be written in a more concise form as

$$\Delta E_n \sim \frac{\hbar}{T_r}\frac{1}{|\sin(((T_m/T_r)S_r - S_m)/(2\hbar) - \pi/2)|}e^{-2S_c/\hbar}, \tag{2.20}$$

(see equation (66) in [35]). As shown in figure 2.6, the semiclassical formula thus derived has reproduced tunnelling splittings obtained by direct numerical diagonalization, not only the slope of the curve but also a sequence of spikes. This analysis tells us that resonance tunnelling can semiclassically be understood as the interference effect among complex classical trajectories. We should note, however, that the semiclassical formula for tunnelling splittings ΔE_n, requires the sum over all possible topologically distinct complex paths connecting two symmetrically located wells (see Appendix B). In this sense, the argument developed in [35] was heuristic at most and lacks evidence showing that the complex trajectories considered there are actually responsible for the creation of spikes.

For the triple-well potential system, we can indeed show that there exist many or even infinitely many topologically independent complex paths because it is possible to solve the classical equa-

[2]Considering the symmetry, we put $S_{\rm rigrt} = S_{\rm left} =: S_r$, $T_{\rm right} = T_{\rm left} =: T_r$.

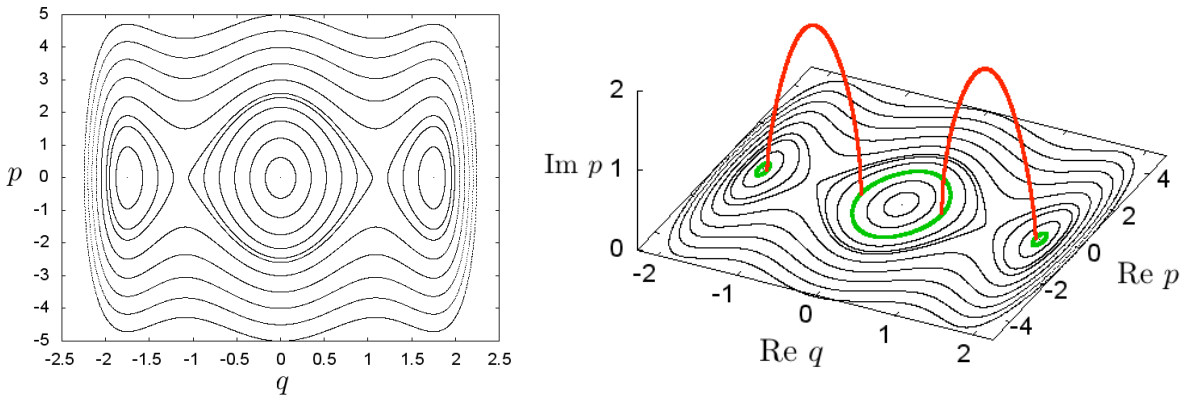

Figure 2.7: (Left)The phase space of the triple-well model (2.14). (Right) A projection of complex path onto the complex phase space.

tions of motion for the triple-well system analytically. Here we only present the final form of the solution,

$$q_{\mathrm{sn}}(t) = \sqrt{\frac{-(\beta-\delta)(a^2+\alpha)+(\alpha-\delta)(a^2+\beta)\mathrm{sn}^2(2\sqrt{-2}Mt,k)}{(\alpha-\delta)\mathrm{sn}^2(2\sqrt{-2}Mt,k)-(\beta-\delta)}}. \tag{2.21}$$

All the details including the derivation and the definition of the parameters are presented in Appendix A.1. The solution is expressed using the Jacobi sn function, so we can specify the divergent points by solving the following equation,

$$\mathrm{sn}^2(2\sqrt{-2}Mt,k) = \frac{\beta-\delta}{\alpha-\delta}. \tag{2.22}$$

From this equation, we understand that the solution of the equations of motion has infinitely many singularities, which implies that there exist infinitely many topologically independent complex classical paths. For the moment, we do not discuss types of singularities, which will be an important issue in the subsequent analysis.

2.4 Normal form Hamiltonian system and complex path

Before discussing the problem addressed above, we will give another class of systems, and introduce a semiclassical analysis made in [43]. The Hamiltonian we here consider takes the form as

$$H(p,q) = H_0(p,q) + V(p,q), \tag{2.23}$$

with

$$H_0(p,q) = \frac{1}{2}(\cos^2 p + \cos^2 q) + a(\cos^2 p + \cos^2 q)^2, \tag{2.24}$$

$$V(p,q) = |b|\{(\cos^4 p + \cos^4 q - 6\cos^2 p \cos^2 q)\cos\phi - 4(\cos^3 p \cos q - \cos^3 q \cos p)\sin\phi\}, \tag{2.25}$$

where a, b, ϕ are real parameters. Here the term H_0 can be rewritten as a form of $\sum a_n(Q^2+P^2)^n$ by introducing new coordinates as $Q = \cos q, P = \cos p$. This form is known as the normal form in the literatures [10, 44, 45]. The Hamiltonian $H(p,q)$ has four local minima at $(p,q) = (\pm\pi/2, \pm\pi/2)$, and a set of equienergy contours surrounds each of them as shown in figure 2.8. Equienergy contour patterns almost look like the same as the pattern typically observed in the Poincaré surface of two-dimensional Hamiltonain systems, or the area-preserving map as shown in figure 2.1. For this reason, the authors of Ref. [43] took this normal form Hamiltonian system to examine the validity of the resonance-assisted tunnelling scenario. Below we review the discussion made in Ref. [43], which invokes many questions and motivates further studies on the complex trajectories in 1-dimensional systems.

The quantum Hamiltonian operator $\hat{H}$ is obtained by quantization of the classical Hamiltonian (2.23) with a symmetrization rule for the product of non-commutative variables

$$f(p)g(q) \to \frac{1}{2}[f(\hat{p})g(\hat{q}) + q(\hat{q})f(\hat{p})] \tag{2.26}$$

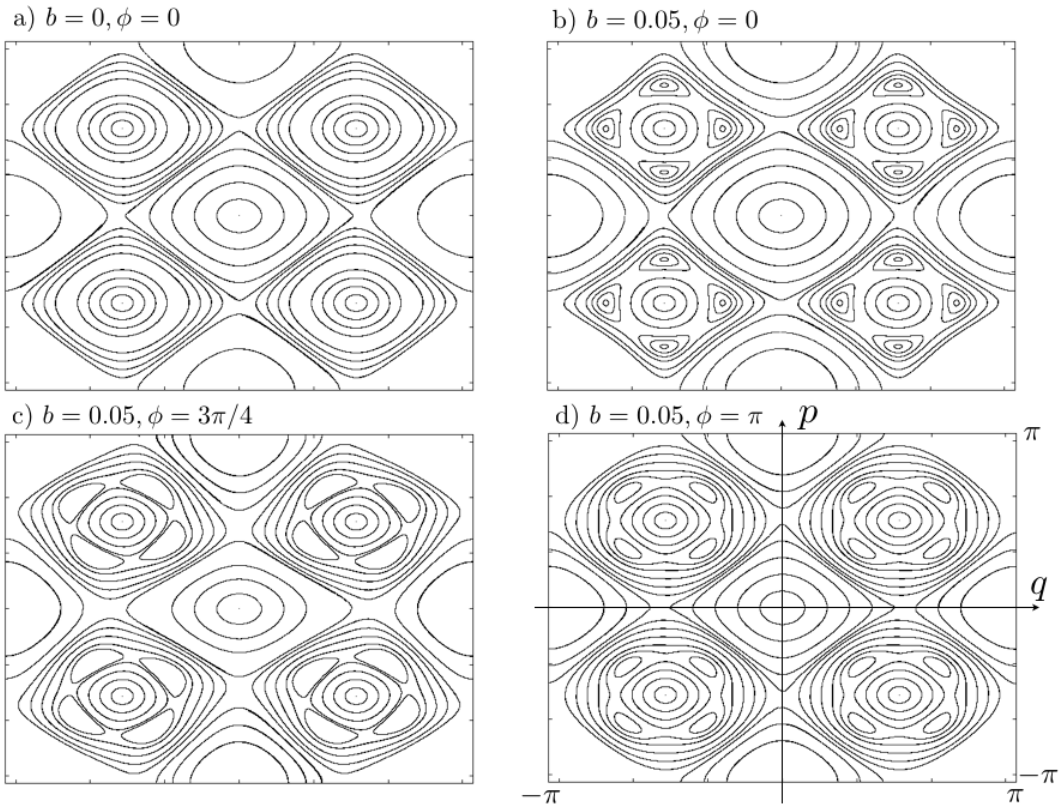

Figure 2.8: The phase space of the Hamiltonian (2.23) with the parameters: a) $a = -0.55, b = 0, \phi = 0$, b) $a = -0.55, b = 0.05, \phi = 0$, c) $a = -0.55, b = 0.05, \phi = 3\pi/4$, d) $a = -0.55, b = 0.05, \phi = \pi$.

where $f(p)$ and $g(q)$ are arbitrary functions of the arguments [46, 47]. The periodicity of the classical Hamiltonian (2.23) allows us to use the Floquet-Bloch theorem [48], so the corresponding quantum system is also defined on the periodical phase space $[-\pi, \pi] \times [-\pi, \pi]$.

The system has two-fold parity with respect to p and q. To define the tunnelling splitting, the authors of Ref. [43] preferred 4 quantum states as follows,

$$|+,+\rangle := \frac{1}{2}(|RU\rangle + |LU\rangle + |LD\rangle + |RD\rangle), \tag{2.27}$$

$$|-,+\rangle := \frac{1}{2}(|RU\rangle - |LU\rangle - |LD\rangle + |RD\rangle), \tag{2.28}$$

$$|+,-\rangle := \frac{\mathrm{i}}{2}(|RU\rangle + |LU\rangle - |LD\rangle - |RD\rangle), \tag{2.29}$$

$$|-,-\rangle := \frac{\mathrm{i}}{2}(|RU\rangle - |LU\rangle + |LD\rangle - |RD\rangle), \tag{2.30}$$

where $|L/R, U/D\rangle$ are eigenstates of harmonic oscillators centered at $(q, p) = (\pm\pi/2, \pm\pi/2)$: $L(R)$ denotes the left (right) column and $U(D)$ the upper (lower) row of the wells, respectively, as shown in figure 2.8. To focus on the tunnelling splitting with respect to the q direction, they considered eigenstates of $\hat{H}$ that have a maximal overlap with the states $|+,+\rangle$ and $|-,+\rangle$. The ΔE_n as a function of $1/\hbar$ is shown in figure 2.9, which exhibits a spike structure as found in the triple-well potential case.

They gave a semiclassical formula, based on a rather phenomenological argument, as

$$\Delta E_n \sim \frac{2\hbar w_{\mathrm{out}}}{\pi} |A_\tau|^2 e^{-S_{\tilde{c}}/2\hbar}, \tag{2.31}$$

where

$$A_\tau = \frac{e^{-S_c/(2\hbar)}}{2\sin((S_{\mathrm{in}} - S_{\mathrm{out}})/(2l\hbar))}. \tag{2.32}$$

Applying this formula, they took a complex path Γ_{bypass} given below:

$$\Gamma_{\mathrm{bypass}} = \Gamma_{\mathrm{in}} + C + \Gamma_{\mathrm{out}} + \tilde{C} + \Gamma'_{\mathrm{out}} + C' + \Gamma'_{\mathrm{in}}, \tag{2.33}$$

which is, as displayed in figure 2.10, given as a combination of real periodic orbits, expressed using

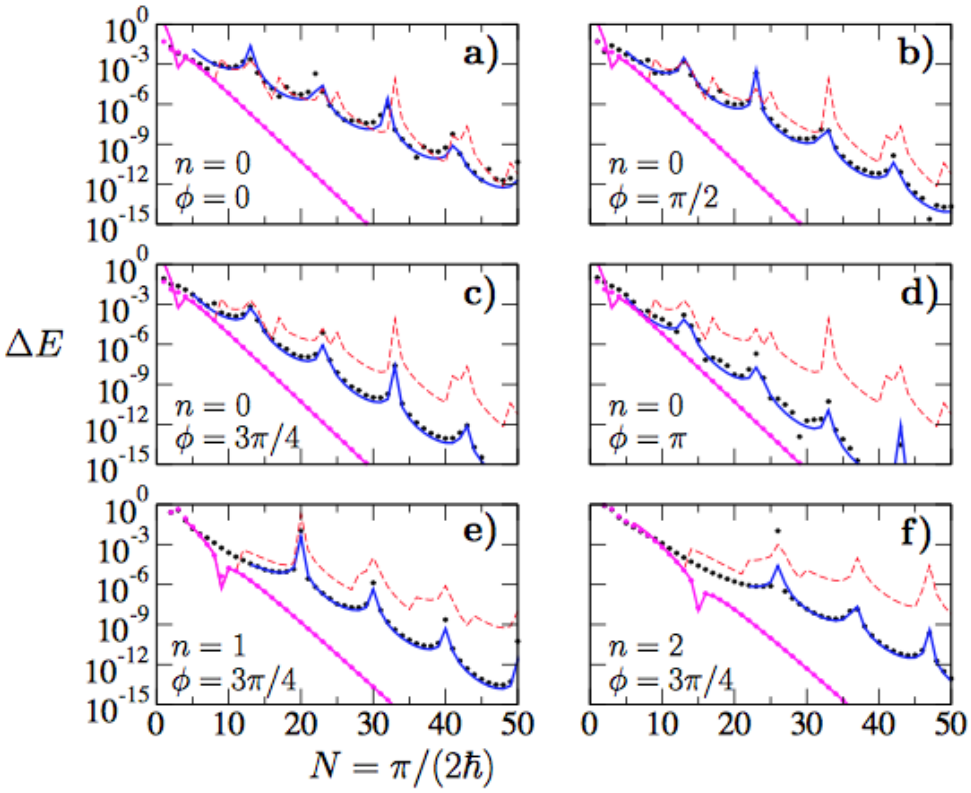

Figure 2.9: The tunnelling splittiing ΔE_n as a function of $\pi/(2\hbar)$, reprinted from [43]. The index n denotes the quantum number. The black dots show the numerical result obtained by direct calculation. The blue curve is obtained by applying the semiclassical formula (2.31). The magenta dots and curves represent the numerical result and the semiclassical evaluation in the case of $b = 0$, respectively. The red dash line shows the calculation based on the RAT scenario [6].

the notation Γ, and complex orbits connecting the two wells, denoted by C. Associated actions are given as

$$S_{\tilde{c}} := \mathrm{Im}\left[\frac{1}{2}\oint_{\tilde{C}} pdq\right], \tag{2.34}$$

$$S_{c} := \mathrm{Im}\left[\frac{1}{2}\oint_{C} pdq\right], \tag{2.35}$$

$$S_{\mathrm{in}} := \oint_{\Gamma_{\mathrm{in}}} pdq, \tag{2.36}$$

$$S_{\mathrm{out}} := \oint_{\Gamma_{\mathrm{out}}} pdq, \tag{2.37}$$

and w_{out} is the frequency of the real outer torus Γ_{out} (see figure 2.10). l is an integer related to the number of hills around each well. In this case, $l = 4$ [43].

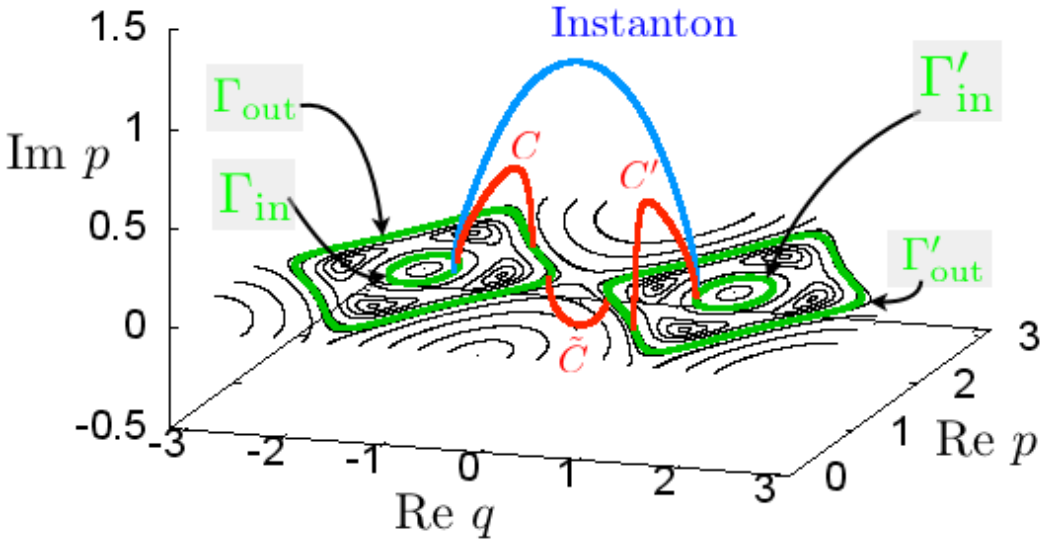

Figure 2.10: The projection of complex paths onto the complex phase space. There appears a bypassing complex path made by a combination of complex paths C, C' and $\tilde{C}$ shown as the red curves and real orbits $\Gamma_{\mathrm{in}}, \Gamma_{\mathrm{out}}, \Gamma'_{\mathrm{in}}$ and Γ'_{out} shown as the green curves. The "instanton" path also exists as shown in the blue curve.

As shown in figure 2.9, the formula taking into account the complex path Γ_{bypass} has well predicted tunnelling splittings between the states associated with symmetrically located wells. What is remarkable in their finding is that not the direct instanton path, shown as a blue curve in figure

2.10, but a bypassing path $\Gamma_{\rm bypass}$ is responsible for reproducing splitting curves and spikes. This is clearly beyond the conventional view of quantum tunnelling, in which the instanton is considered to be the most dominant contributor to tunnelling between wells.

The existence of such a bypassing path reminds us of the resonance-assisted tunnelling scenario, where nonlinear resonances assist the tunnelling transport from the inside to the outside of the well. We should however recall that nonlinear resonances appearing in the phase space of, not in the 1-dimensional but only in multi-dimensional systems and the energy wells observed in figure 2.8 in 1-dimensional systems have completely different origins, so apparent similarity in the pattern of phase space might mislead us. For this reason, their result has, strictly speaking, nothing to do with the resonance-assisted tunnelling, which can appear only in multi-dimensional systems. Nevertheless, it would be a very important discovery that non-instanton complex path giving the dominant contribution actually exists.

It should be remarked that even though they have actually predicted tunnelling splittings using the complex paths heuristically found, we cannot eliminate the possibility that the agreement they obtained was merely accidental. This is because, as is the case of the triple-well potential system, there might exist infinitely many candidate complex paths in their system. We can indeed confirm this by examining solutions of the following simpler Hamiltonian:

$$H(p,q) = \frac{p^2}{2} + \frac{q^2}{2} + \epsilon\left(\frac{p^2}{2} + \frac{q^2}{2}\right)^2 + \eta p^2 q^2. \tag{2.38}$$

The phase space of this model is very similar to a quarter part of the phase space of the system (2.25) (see figure A.1). The exact solution of this model is obtained in Appendix. A.3 as

$$q(t) = \left(\frac{1}{2}\left(\frac{A^{1/2}}{\epsilon+\eta}\sin\theta(t) - \frac{1}{\epsilon+\eta} + \left(\frac{A}{-\eta(\epsilon+\eta)}\right)^{1/2}\cos\theta(t)\right)\right)^{1/2}, \tag{2.39}$$

where $\theta(t)$ is expressed using the Jacobi sn function. As is the triple-well case, we can easily see

that the divergent points of classical trajectories are obtained by solving the equation

$$\mathrm{sn}^2(\sqrt{\frac{4\epsilon A}{\epsilon+\eta}}Mt, k) = \frac{z_\beta - z_\delta}{z_\alpha - z_\delta}. \tag{2.40}$$

Here each parameter is defined in Appendix A.3. The exact solution tells us that there exist infinitely many singularities periodically located in the time plane of $q(t)$. It is possible to see the relation to the original system (2.25) by performing the change of variable as $q \to \cos q$, which keeps the singularity structure of the solution, meaning that the solution of the original system also has infinitely many singularities, and infinitely many topologically independent complex paths.

Chapter 3

Semiclassical formula of tunnelling splitting and action integral

3.1 Semiclassical formula for the tunnelling splitting

In this section, we introduce a semiclassical formula on which we will rely throughout the following analysis. In Ref. [35], a semiclassical trace formula for tunnelling splittings has been derived and it was shown to work well in a symmetric triple-well potential system. Below we briefly explain the formula to show how *complex classical orbits* come into play in determining tunnelling splittings (see more details in Appendix B and Ref. [35]).

Let us consider a 1-dimensional classical Hamiltonian $H(p, q)$ having reflection symmetry with respect to the canonical variables p and q:

$$H(p, q) = H(-p, -q). \tag{3.1}$$

The energies $E_n^{\pm}$ and the associated eigenstates $|\phi_n^{\pm}\rangle$ of the corresponding quantum model are given by

$$\hat{H}|\phi_n^{\pm}\rangle = E_n^{\pm}|\phi_n^{\pm}\rangle, \tag{3.2}$$

where $\hat{H} = H(\hat{p}, \hat{q})$ with $\hat{p}$ and $\hat{q}$ being the canonical operators associated with p and q, respectively. The superscripts $\pm$ stand for the symmetric/antisymmetric states and tunnelling manifests itself through the splittings $\Delta E_n = E_n^- - E_n^+$.

In Ref. [35], a semiclassical formula for the energy splitting ΔE_n has been derived as

$$\Delta E_n \sim \frac{\hbar}{2T} \sum_{\mathrm{cl}} (-1)^{\mu+1} e^{\mathrm{i}S_{\mathrm{cl}}/\hbar}, \tag{3.3}$$

where the sum is taken over all the classical paths with energy $E \sim E_n^{\pm}$ such that $q(T) = -q(0)$ and $p(T) = -p(0)$ for a given time interval T. Although the time interval T appears explicitly in the formula, it has been shown in Ref. [35] that the right-hand side of (3.3) becomes independent of T as long as $\mathrm{Im}\, T$ is taken to be large enough compared to the typical (real) period of the classical system.

The quantities S_{cl} and μ denote the classical action of the path Γ

$$S_{\mathrm{cl}} = \int_{\Gamma} p(q) dq \ \ (=: S_{\Gamma}), \tag{3.4}$$

and the Maslov index [49], respectively. The function $p(q)$ is defined by

$$H(p, q) = E, \tag{3.5}$$

where $E \simeq E_n^{\pm}$ and we will always left implicit the dependence on E. Since there exist no real classical paths connecting two classically disjointed regions, the path Γ runs in the complex plane.

Formula (3.3) comes from the saddle point approximation, therefore, in order to apply it, two steps can be identified. The first one is to list all the possible complex paths that could contribute to the sum in the formula and the second step is to select in this list of candidates those that actually contribute to ΔE_n. As far as the first step is concerned, in general, even in the simplest models such as double-well potential systems, the classical solutions with appropriate boundary conditions occur in families of infinite numbers and it is a non-trivial task to enumerate all these stationary paths. Even after enumerating all the possible candidates, it is known that not all of them do not necessarily remain as final contributions. This is because the Stokes phenomenon occurs in the

complex plane, and some saddles have to be excluded from the final contribution. The second step we should consider is therefore to find a proper way of handling the Stokes phenomenon.

In Ref. [35] and as actually shown in the previous sections, the formula (3.3) was satisfactorily tested in some standard models with a procedure for achieving the first step that does not guarantee that all the possible complex stationary path were considered. To justify the adopted method and to have a better control on the approximations, we need to establish a systematic way, based on more rigorous grounds, to achieve step one. Our subsequent argument will be focused mainly on this step. Concerning the second step, although the Stokes phenomenon could be now captured as a well recognised object [50–52] and even within the scope of rigorous arguments thanks to recent progress of the so-called *exact WKB analysis*, or *resurgent theory* [53], we will not take into account the Stokes phenomenon based on such recent developments, rather treat the Stokes phenomenon in a heuristic way, as explained below.

As is easily seen, classical actions associated with complex paths have imaginary parts, and the complex path(s) with the most dominant weight are supposed to have minimal imaginary action. Note that such an argument of course holds only after handling the Stokes phenomenon in an appropriate manner. Our task here is therefore to enumerate all the possible candidate complex paths and then to specify the complex path with the smallest imaginary action out of the candidates.

The strategy for the first step is to examine the *fundamental group* of the Riemann surface R of the function $p(q)$ since the fundamental group provides the topological independent paths on a given surface. In addition to such information we also need to specify singularities of the function $p(q)$. This is because, by virtue of Cauchy theorem, the value of the classical action (3.4) is affected when a continuous deformation of Γ crosses singularities.

3.2 Action integral and topology of complex trajectory

Each action integral is evaluated along the corresponding complex classical path. We may deform the classical path continuously unless the classical path crosses over singularities. However, as shown in the previous chapter, infinitely many singularities on the time plane exist in the systems examined here, and correspondingly there appear infinitely many topologically independent paths.

It would be impossible to handle infinitely many paths in numerical computations, so we need a certain analytical argument.

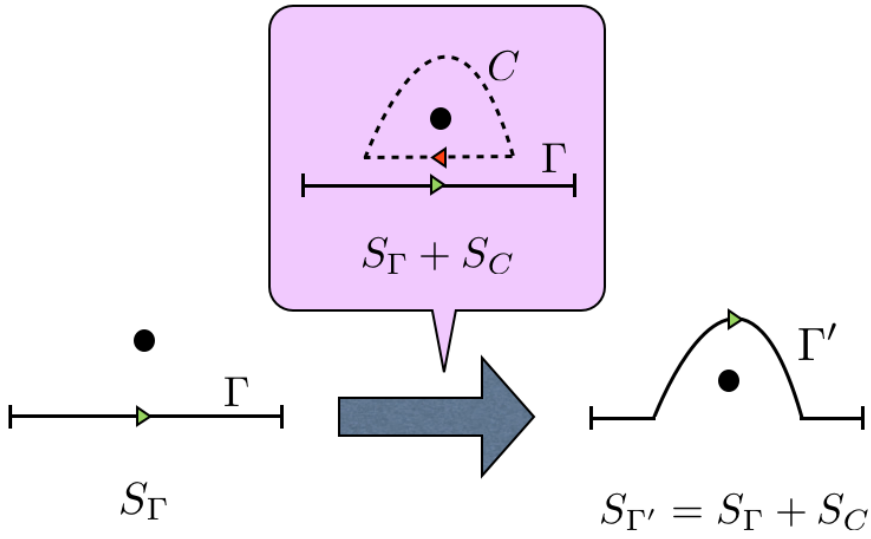

Figure 3.1: Deforming of the path Γ to the path Γ' and the corresponding action integral $S_\Gamma, S_{\Gamma'}$. The black dot shows a singularity point. C is a closed loop encircling the singularity.

Our strategy to enumerate topologically distinct paths is follows. Suppose a complex path denoted by Γ connecting two end points (see figure 3.1), and the associated action integral S_Γ. If a given path Γ is deformed continuously to pass through a singularity, due to the Cauchy's theorem, the action $S_{\Gamma'}$ of the deformed path is given by the sum of the original action S_Γ plus the action S_C around the singularity (see figure 3.1). The action S_C is evaluated along a small loop encircling the singularity. Hence, our task to enumerate topologically independent paths could be reduced to specifying closed loops encircling each singularity. In the systems considered here, singularities are either poles or branch points at most. If branch points appear, we have to consider multiple Riemann sheets and the topology of the path is characterised by the Riemann sheet structure.

As a simple example, let us consider a function $f(z) = \sqrt{z}$. The function is double-valued except for a branch point $z = 0$. After drawing a branch cut from $z = 0$ to $z = \infty$, we can consider the the Riemann sheet associated with the function $f(z)$ (see figure 3.2). Each sheet can be projected onto a Riemann sphere, and then the Riemann spheres are deformed after opening the branch cut to form a sphere as shown in figure 3.3. The resulting surface is called the Riemann

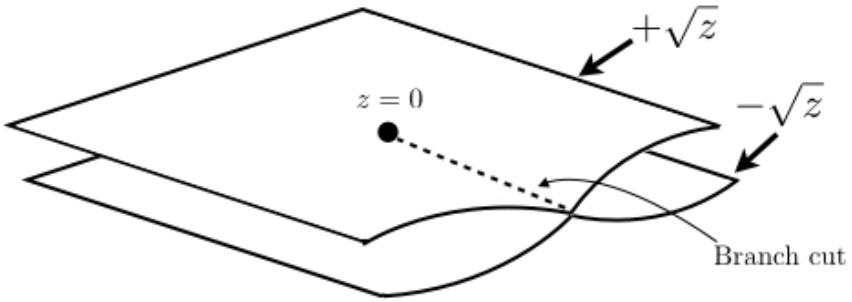

Figure 3.2: Complex z-plane of a function $\sqrt{z}$. Dashed line is a branch cut.

surface. We further regard the branch points as small holes, and deform it to have a cylinder space (see also shown in figure 3.4). We could then recognise that there exists a single loop on the Riemann surface for the function $f(z) = \sqrt{z}$. It is obvious that counting independent loops around essential singularities is impossible, so hereafter we restrict our Hamiltonian to those expressed as polynomial functions of p and q. This condition makes it possible to enumerate all possible independent loops.

3.3 Fundamental group of Riemann surfaces of algebraic functions

In this section, we show how the fundamental group of the Riemann surface R of the function $p(q)$ helps to construct the path Γ along which the classical action (3.4) is computed. In what follows, we assume that our Hamiltonian $H(p, q)$ is expressed as a polynomial function of p and q and the polynomial is irreducible. The former condition allows to obtain the complete list of the complex paths contributing to the semiclassical sum (3.3) and the latter one ensures that the Riemann surface of the function $p(q)$ is connected.

H being a polynomial, the function $p(q)$ defined by (3.5) is an algebraic function and therefore

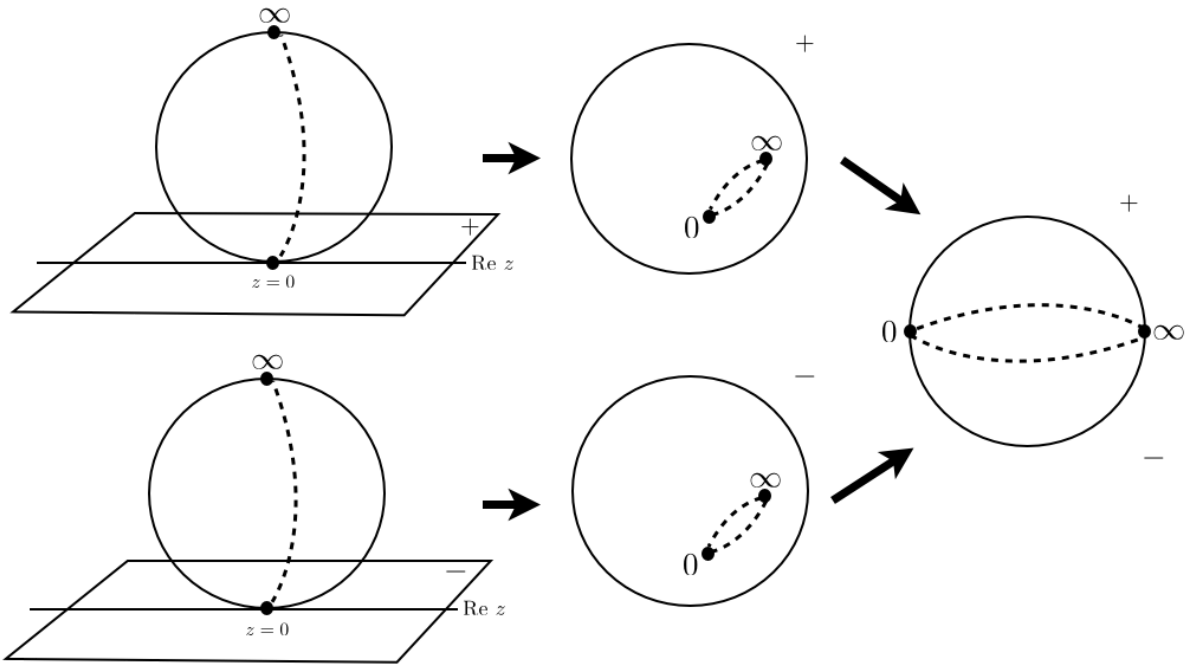

Figure 3.3: Deformation of Riemann spheres to a sphere.

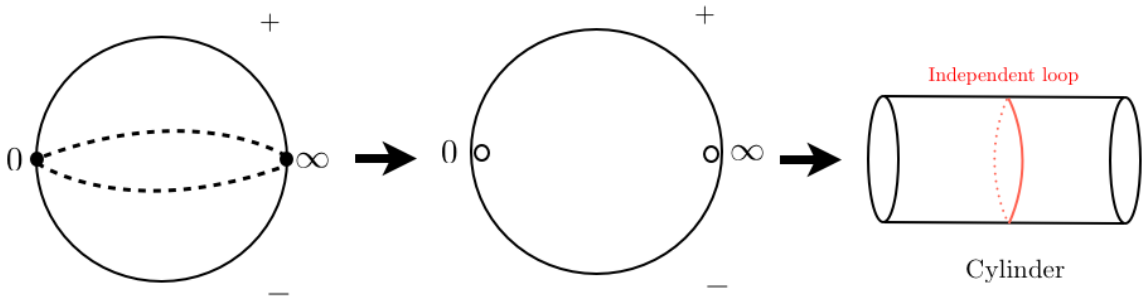

Figure 3.4: Deforming the Riemann surface of a function $\sqrt{z}$ to a cylinder space. The red curve is the only topologically independent loop on the Riemann surface.

has at most finitely many singularities [1] [55] that are points where $p(q)$ has a pole or a branch point. Since our Riemann surface R is constructed from an algebraic function and assumed to be irreducible, it is homeomorphic to a surface of a finite genus g, or g-fold torus for short, accompanied with finite number of holes associated with singularities of the function under consideration. The genus of the surface is given by the formula $g = w/2 - d + 1$, where w is the ramification index and d is the highest degree of p in the polynomial in question. Especially, w is equal to the number of branch points if all branch points are square-root type, i.e., the function is double-valued near each branch point. For example, in multi-well potential systems discussed in sections 4.1 and 4.2, and the normal form Hamiltonian system in section 4.4 as well, $p(q)$ is shown to be double-valued functions near each branch point.

The fundamental group on the Riemann surface is introduced as the group whose elements are identified through homotopy equivalence of curves on the surface. For the g-fold torus, there exist $2g$ independent homotopically equivalent loops, and following the convention we call the half of them α_i-loop and the rest β_i-loop ($1 \leq i \leq g$). The loops α_i and β_i are often called *homology basis* in the literature [55].

When computing the action integral (3.4) one must include the contribution of singularities which could provide non-zero residues, when deforming Γ. This means that the associated fundamental group should be replaced by the one incorporating singularities of the function $p(q)$. The Seifert-Van Kampen theorem tells us that the fundamental group for a surface with holes is obtained as the product of the fundamental group for the original g-fold torus and that of a sphere with m holes, where m is the number of holes [56], which appear as either poles or branch points in the present situation. We call the loop encircling a hole the γ_i loop ($1 \leq i \leq m$), again following the convention. The loop γ_i here is taken to be a small closed loop around each hole (see figure 3.5).

We note also from the Seifert-Van Kampen theorem that the elements α_i, β_i and γ_i of the

[1] The number of singularities of an algebraic function is finite. The reason is that, if the number of singularities is infinite, let us consider a projection of singularities onto the Riemann sphere (is compact space) and application of the Bolzano-Weierstrass theorem, there exists at least one accumulation point of singularities. However, the algebraic function cannot have accumulation points of singularities [54].

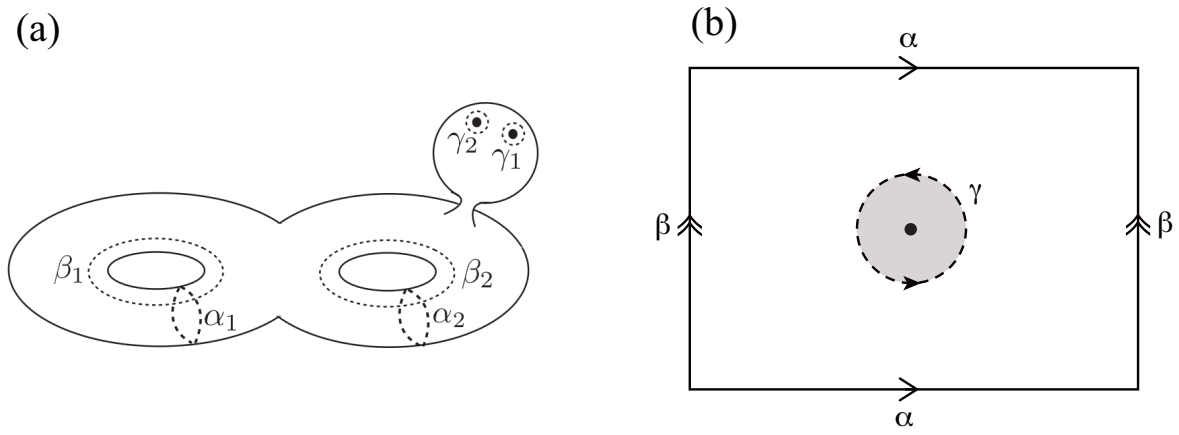

Figure 3.5: (a) An example of the Riemann surface. Here the case for the 2-fold torus with two holes is presented. Homology bases of the fundamental group are shown as $\alpha_1, \alpha_2, \beta_1, \beta_2, \gamma_1$ and γ_2. (b) A graphical proof for the relation (3.6). A simple torus with a hole is here assumed.

fundamental group satisfy a relation,

$$\prod_i \alpha_i \beta_i \alpha_i^{-1} \beta_i^{-1} = \prod_i \gamma_i \tag{3.6}$$

implying that all the loops α_i, β_i and γ_i are not independent with each other. We hereafter assume that one of γ_i-loops, say γ_m, is expressed in terms of the other loops. We just graphically show in figure 3.5 why the relation (3.6) follows in the simplest situation where a simple torus with $g = 1$ is connected with a sphere with a hole.

Using the elements of the fundamental group, we can now enumerate all the topologically distinct paths obtained from a reference path Γ_0. More concretely, for an arbitrarily chosen reference path Γ_0 with the fixed initial and final ends in the q-plane, topologically independent paths associated with the reference path Γ_0 are expressed as

$$\Gamma = \Gamma_0 + \sum_{i=1}^{g} n_{\alpha_i} \alpha_i + \sum_{i=1}^{g} n_{\beta_i} \beta_i + \sum_{i=1}^{m-1} n_{\gamma_i} \gamma_i, \tag{3.7}$$

where $n_{\alpha_i}, n_{\beta_i}$ and n_{γ_i} are integers and will be called winding numbers hereafter. In what follows we apply the scheme formulated in this way to a couple of concrete examples, some of them are the systems already well studied.

Chapter 4

Applications

4.1 Double-well potential case

As a simple example, we first discuss a double-well potential system:

$$H(p,q) = \frac{p^2}{2} + V(q), \tag{4.1}$$

$$V(q) = E + (q-q_1)(q-q_2)(q-q_3)(q-q_4). \tag{4.2}$$

Here q_i $(1 \leq i \leq 4)$ are real parameters satisfying $q_1 < q_2 < q_3 < q_4$ and E is the total energy. We further assume that the potential function is symmetric, that is $q_1 = -q_4, q_2 = -q_3$ (see figure 4.1) in accordance with (3.1) even though this symmetry condition is not relevant for topological considerations. From (3.5) we find

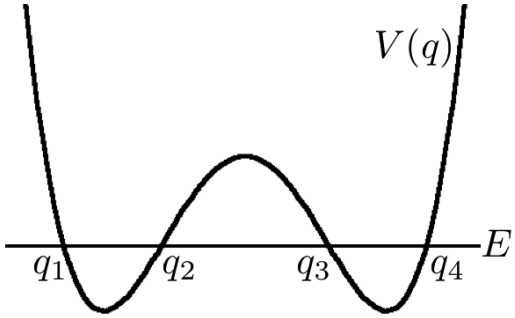

Figure 4.1: The double-well potential $V(q)$.

$$p(q) = \pm\sqrt{-2(q-q_1)(q-q_2)(q-q_3)(q-q_4)}. \tag{4.3}$$

The function $p(q)$ has four branch points at $q = q_i$ $(1 \leq i \leq 4)$, which are all located on the real axis and one can choose the intervals $[q_1, q_2]$ and $[q_3, q_4]$ as two cuts defining a Riemann surface with two leaves. As shown in figure 4.2, we project each leaf onto the Riemann sphere and continuously deform two spheres by opening the branch cuts. We finally get a simple torus with $g = 1$ with holes associated with the singularities.

The homology basis of the fundamental group in this case is composed of the loops α, β, which are homotopically independent loops on the torus, together with the loops encircling singularities. In addition to branch points at $q = q_i$ $(1 \leq i \leq 4)$, there exist poles at $q = \pm\infty$, and we denote the loops associated with singularities by γ_i $(1 \leq i \leq 4)$ and $\gamma^{(\pm\infty)}$, respectively (see figure 4.3). Relations (3.6) allow to express, γ_4, say, as a product of the other loops considered to be independent. As shown in the previous section, with fixed initial and final end points, the variety of distinct values of the action integral is given based on the formula (3.7).

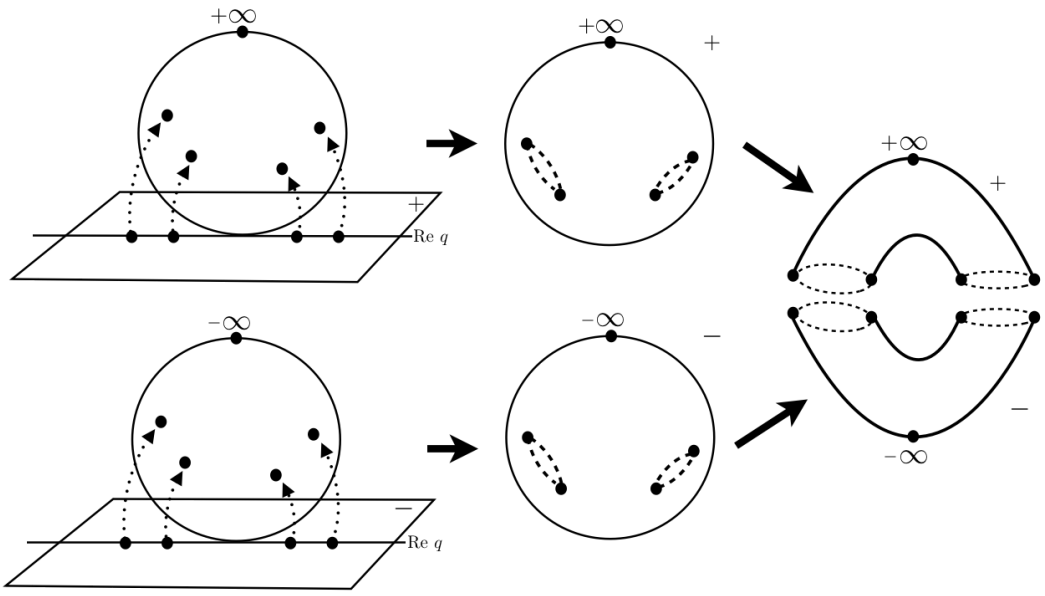

Figure 4.2: Deformation of Riemann spheres to a torus is shown in the double-well potential case. The black dots and the dashed lines represent branch points and branch cuts, respectively. $\pm$ signs show the branches of $p(q)$.

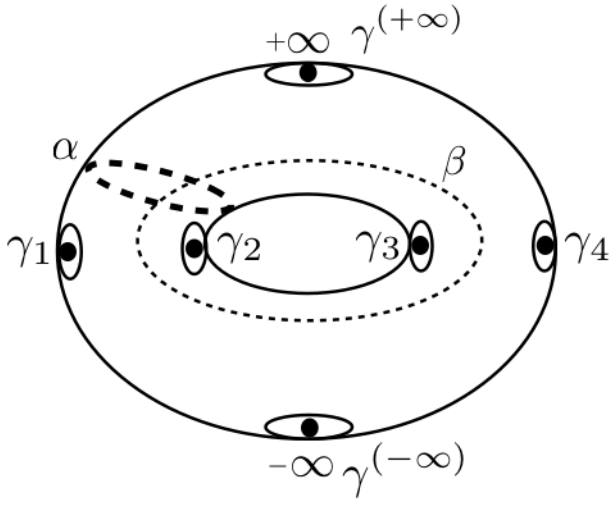

Figure 4.3: Homology basis of the fundamental group for the torus $\mathcal{T} \setminus \{q_1, q_2, q_3, q_4, +\infty, -\infty\}$.

Recall the semiclassical formula (3.3) for the tunnelling splitting requires the complex paths connecting the points symmetrically located in the q-plane then we may take Γ_0 to connect q_2 and $q_3 = -q_2$. Without loss of generality, we can obtain arbitrary symmetric paths from the path connecting the branch points q_2 and q_3 by shifting both initial and final points simultaneously keeping the symmetry condition. All the topologically distinct paths, taking into account the contribution from divergent singularities, are then written as

$$\Gamma = \Gamma_0 + n_\alpha \alpha + n_\beta \beta + \sum_{i=1}^{3} n_{\gamma_i} \gamma_i + n^{(+\infty)} \gamma^{(+\infty)} + n^{(-\infty)} \gamma^{(-\infty)}, \tag{4.4}$$

where $n_\alpha, n_\beta, n_{\gamma_i}$ and $n^{(\pm\infty)}$ are winding numbers of each loop.

As is discussed below, it is important to specify the α and β loops explicitly when one actually evaluates the action integrals, while we can freely move and deform the α and β loops and the locations are not relevant within the argument of the fundamental group (see figure 3.5).

For simplicity, we take two independent loops α and β on the torus in such a way that each branch in the α loop runs along the real q-axis with encircling the two branch points q_1 and q_2, and in the same way the β loop encircles the two branch points q_2 and q_3 (see figure 4.4). By taking

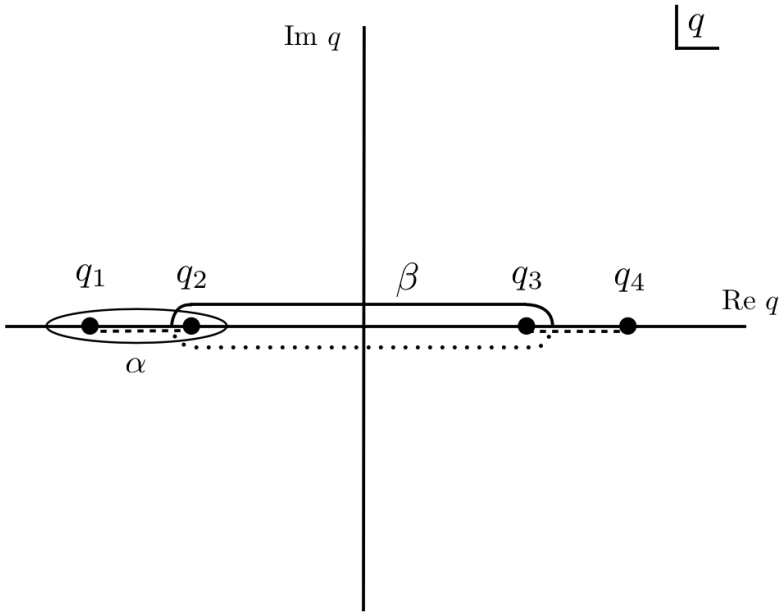

Figure 4.4: α, β loops taken as integration contours on the q plane.

the loops α and β in this manner, the action integral for the α loop turns out to be real valued and that for the β loop purely imaginary valued. As shown in Appendix C, the action integrals for γ_i $(i = 1, 2, 3)$ vanish. We then reach the expression for the total action integral after summing over all the contributions as

$$S_\Gamma = S_{\Gamma_0} + n_\alpha S_\alpha + n_\beta S_\beta + n^{(+\infty)} S^{(+\infty)} + n^{(-\infty)} S^{(-\infty)}, \tag{4.5}$$

where

$$\begin{aligned} S_{\Gamma_0} &:= \int_{q_2}^{q_3} pdq, \\ S_\alpha &:= \oint_\alpha pdq = 2\int_{q_1}^{q_2} pdq, \\ S_\beta &:= \oint_\beta pdq = 2\int_{q_2}^{q_3} pdq, \\ S^{(\pm\infty)} &:= \oint_{\gamma^{(\pm\infty)}} pdq. \end{aligned} \tag{4.6}$$

Now we show that S_α and $S^{(\pm\infty)}$ are not independent and actually related with each other. To see this, we rewrite as $S_L = S_\alpha$ for the left-side well, and introduce the action integral for the right-side well as

$$S_R := 2\int_{q_3}^{q_4} pdq. \tag{4.7}$$

As illustrated in figure 4.5, the integration contour specifying the action integral S_L is continuously deformed and split into the ones associated with the action integrals $S^{(+\infty)}$ and S_R. This leads to the relation

$$S_L = S_R - S^{(+\infty)}, \tag{4.8}$$

where the minus sign in front of $S^{(+\infty)}$ comes from the phase of p (see Appendix D). From the symmetry of the potential function, it is obvious that $S_L = S_R$ holds. This automatically gives $S^{(+\infty)} = 0$, which can also be confirmed by the direct calculation of the residue at $q = +\infty$ (also see Appendix D). From this observation, the candidates of action integrals finally take a simple form as

$$S_\Gamma = S_{\Gamma_0} + n_\alpha S_\alpha + n_\beta S_\beta. \tag{4.9}$$

Next we turn our attention to the most dominant complex path in the semiclassical formula (3.3). Since classical action integrals under consideration are complex valued, the most dominant contribution is supposed to come from the complex classical orbit(s) with minimal imaginary action $\mathrm{Im}\, S$. In the present situation, the α loop contribution is real valued, so the imaginary part of action integral is written as

$$\mathrm{Im}\, S_\Gamma = \mathrm{Im}\, S_{\Gamma_0} + n_\beta \mathrm{Im}\, S_\beta. \tag{4.10}$$

This may take arbitrarily large negative values as n_β is allowed to be any integer, positive or negative, meaning that imaginary action can become arbitrarily small. However, it is obvious that

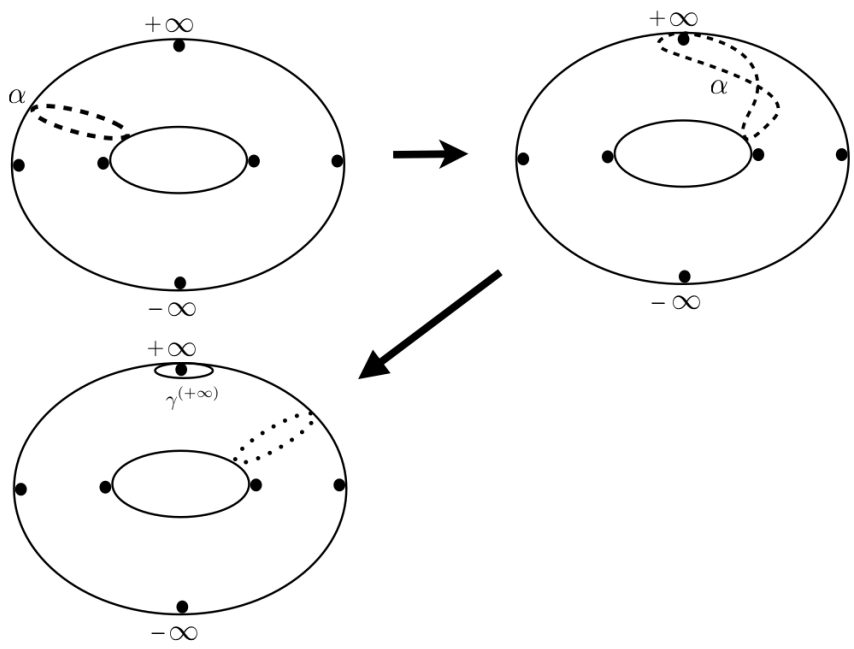

Figure 4.5: Deformation of the α loop in the left well. It splits into a combination of the α loop in the right well and a loop around $+\infty$.

the orbits with negative imaginary action give rise to exponentially large contributions, which are not physically accepted, so should be dropped from the final contributions.

Excluding unphysical contributions out of necessary ones could be done by handling the Stokes phenomenon properly. This would therefore be a matter of issues which should be closely discussed in order to make our theory self-consistent. However, as mentioned in section 3.1, we here treat the Stokes phenomenon only in a heuristic manner. The principle we adopt is based on the behaviour of imaginary action as time proceeds. From the Hamiltonian equations of motion, $dq = pdt$ follows, which results in $\int pdq = \int p^2 dt$. We then have [1]

$$\mathrm{Im}\, S = \int -\mathrm{Im}\, p^2 \mathrm{Im}\, dt. \tag{4.11}$$

and in order to get $\mathrm{Im}S > 0$ we will choose a parametrisation such that $\mathrm{Im}\, dt < 0$. In this choice, $\mathrm{Im}\, S$ becomes negatively large with increase in $\mathrm{Im}\, dt$ in a monotonic way.

If one applies this rule, which will also be used in the examples discussed below, Γ_0 is given as

[1] p has only imaginary part when one integrates it along to the β loop.

a trajectory passing through the potential barrier only once, that is a half cycle of the β loop, and the smallest imaginary action is just

$$\mathrm{Im}\, S_\Gamma = \frac{1}{2}\, S_\beta. \tag{4.12}$$

This is nothing but the imaginary action for the so-called instanton path. From the expression (4.9), the corresponding real part turns out to be

$$\mathrm{Re}\, S_\Gamma = n_\alpha S_\alpha. \tag{4.13}$$

Since branch points are turning points and α, β loops encircle the two branch points, we find that the Maslov index is equal to $\mu = 2n_\alpha + 1$. Incorporating the semiclassical quantization condition $S_\alpha = (1/2 + N)2\pi\hbar$, the formula (3.3) can now be explicitly written as

$$\begin{aligned}
\frac{\hbar}{2T} e^{-S_\beta/2\hbar} \sum_{n_\alpha} (-1)^{2n_\alpha+2} e^{i n_\alpha S_\alpha/\hbar} &= \frac{\hbar}{2T} e^{-S_\beta/2\hbar} \sum_{n_\alpha} (-1)^{2n_\alpha+2} e^{i n_\alpha (1/2+N)2\pi\hbar/\hbar} \\
&= \frac{\hbar}{2T} e^{-S_\beta/2\hbar} \sum_{n_\alpha} (-1)^{2n_\alpha+2} e^{i n_\alpha \pi} e^{i n_\alpha N 2\pi} \\
&= \frac{\hbar}{2T} e^{-S_\beta/2\hbar} \sum_{n_\alpha} (-1)^{2n_\alpha+2} (-1)^{n_\alpha}.
\end{aligned} \tag{4.14}$$

Here the sum over the winding number n_α is cancelled except for the case $n_\alpha = 0$. From these arguments we finally obtain the formula

$$\Delta E \sim \frac{\hbar}{2T} e^{-S_\beta/2\hbar}. \tag{4.15}$$

This is nothing but the well known formula in the instanton theory (see equation (2.10)), and also coincides with the result rederived in [35].

4.2 Triple-well potential case

As a next example, we consider a triple-well potential system:

$$H(p,q) = \frac{p^2}{2} + V(q), \tag{4.16}$$

$$V(q) = E + (q-q_1)(q-q_2)(q-q_3)(q-q_4)(q-q_5)(q-q_6),$$

where the parameters q_i $(1 \leq i \leq 6)$ are all real and satisfy the conditions $q_1 < q_2 < \cdots < q_6$. We again assume the conditions $q_1 = -q_6, q_2 = -q_5, q_3 = -q_4$ in order to develop the semiclassical analysis for the tunnelling splitting (see figure 4.6).

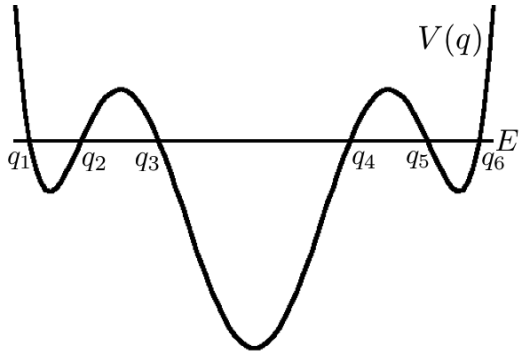

Figure 4.6: The triple-well potential $V(q)$.

In the same way as the double-well case, we obtain $p(q)$ as

$$p(q) = \sqrt{-2(q-q_1)(q-q_2)(q-q_3)(q-q_4)(q-q_5)(q-q_6)}.$$

The function $p(q)$ has now six branch points on the real axis. The associated Riemann surface of $p(q)$ is homeomorphic to a 2-fold torus with small holes associated with branch points and poles (see figure 4.7). The homology basis of the fundamental group is composed of the loops α_i and β_i $(i = 1, 2)$ on the 2-fold torus and γ_i $(1 \leq i \leq 6)$ and $\gamma^{(\pm\infty)}$, each of which is a small loop encircling the corresponding singularity. We illustrate in figure 4.8 the elements of the fundamental group in this case.

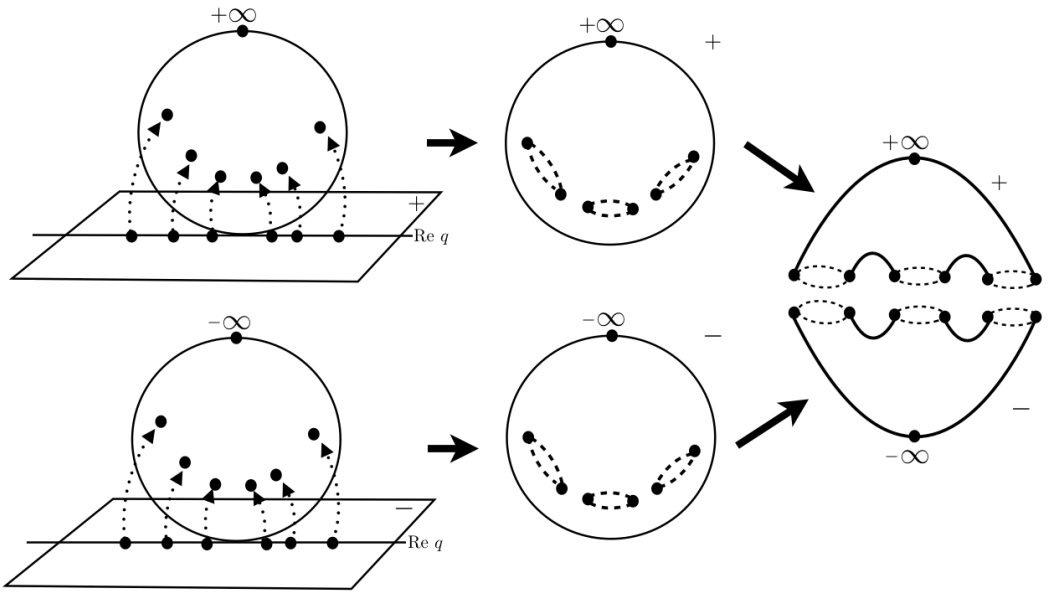

Figure 4.7: Deformation of Riemann spheres to a torus is shown in the triple-well potential case. The black dots and the dashed lines represent branch points and branch cuts, respectively. $\pm$ signs show the branches of $p(q)$.

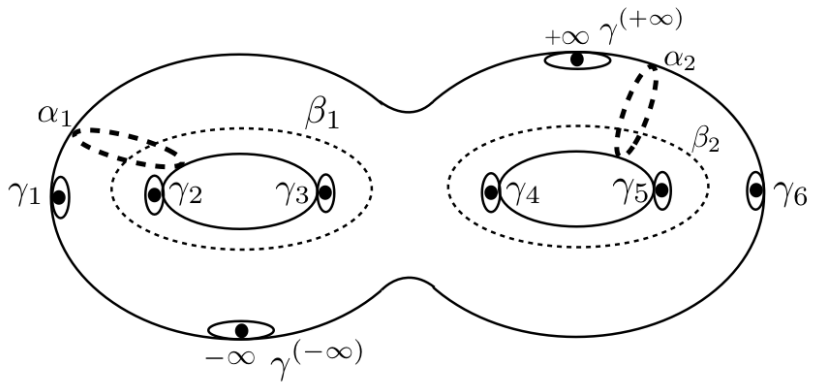

Figure 4.8: Homology basis for the surface $\mathcal{T}\#\mathcal{T} \setminus \{q_1, q_2, q_3, q_4, q_5, q_6, +\infty, -\infty\}$.

To discuss the tunnelling splitting between the states localized at the left- and right-wells, let Γ_0 be a path connecting the branch points q_2 and $q_5 = -q_2$. The integration contour is given by a combination of these loops as follows, keeping in mind that γ_6 is a product of the other loops,

$$\begin{aligned}\Gamma = \Gamma_0 \quad &+ \quad \sum_{i=1}^{2} n_{\alpha_i}\alpha_i + \sum_{i=1}^{2} n_{\beta_i}\beta_i \\ &+ \quad \sum_{i=1}^{5} n_{\gamma_i}\gamma_i + n^{(+\infty)}\gamma^{(+\infty)} + n^{(-\infty)}\gamma^{(-\infty)},\end{aligned} \tag{4.17}$$

where $n_\alpha, n_\beta, n_{\gamma_i}$ and $n^{(\pm\infty)}$ are winding numbers of each loop. Again using the result shown in Appendix C, the action integrals for γ_i $(i = 1, 2, \cdots, 5)$ all vanish, and we reach the expression for the total action integral contributions,

$$S_\Gamma \quad = \quad S_{\Gamma_0} + \sum_{i=1}^{2} n_{\alpha_i} S_{\alpha_i} + \sum_{i=1}^{2} n_{\beta_i} S_{\beta_i} + n^{(+\infty)} S^{(+\infty)} + n^{(-\infty)} S^{(-\infty)}, \tag{4.18}$$

where

$$\begin{aligned} S_{\Gamma_0} &:= \int_{q_2}^{q_5} pdq, \\ S_{\alpha_1} &:= \oint_{\alpha_1} pdq = 2\int_{q_1}^{q_2} pdq, \\ S_{\alpha_2} &:= \oint_{\alpha_2} pdq = 2\int_{q_5}^{q_6} pdq, \\ S_{\beta_1} &:= \oint_{\beta_1} pdq = 2\int_{q_2}^{q_3} pdq, \\ S_{\beta_2} &:= \oint_{\beta_2} pdq = 2\int_{q_4}^{q_5} pdq, \\ S^{(\pm\infty)} &:= \oint_{\gamma^{(\pm\infty)}} pdq. \end{aligned} \tag{4.19}$$

As done in the double-well potential case, we next show that these action integrals are not independent. As illustrated in figure 4.9, the integration contours specifying S_{α_1} and S_{α_2} are continuously deformed and split into the ones associated with the action integrals $S^{(+\infty)}$ and S_C.

Here S_C stands for the action integral for the central well,

$$S_C := 2\int_{q_3}^{q_4} pdq. \tag{4.20}$$

Rewriting the notation as $S_L = S_{\alpha_1}$ and $S_R = S_{\alpha_2}$ to make clear that S_{α_1} and S_{α_2} are action integrals for the left- and right-side wells, we obtain the relation

$$S_C = S_L + S_R + S^{(+\infty)}. \tag{4.21}$$

This relation can also be confirmed in the direct calculation presented in Appendix D. A similar relation holds for $S^{(-\infty)}$ except that the sign in front of $S^{(-\infty)}$ is minus.

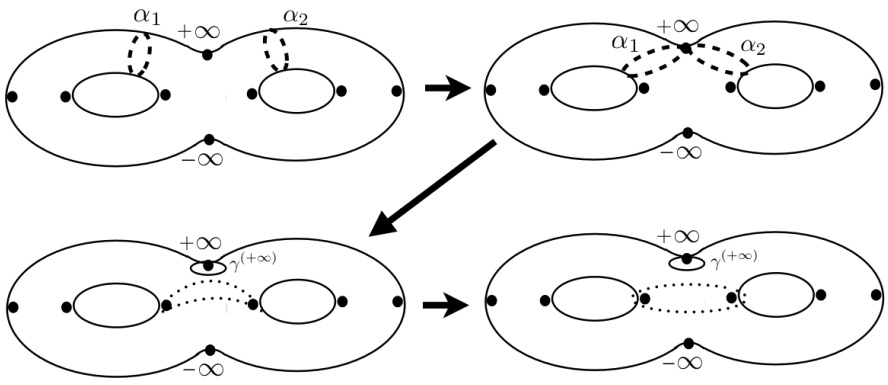

Figure 4.9: Deformation of the α_1 and α_2 loops in the left- and right-wells. They split into a combination of the loop for the central well and a loop encircling $+\infty$.

The symmetry of the potential function leads to the relations $S_R = S_L$, and $S_{\beta_1} = S_{\beta_2}$. As a result, all the possible classical action integrals are simply expressed as

$$S_\Gamma = S_{\Gamma_0} + n_L S_L + n_C S_C + (n_{\beta_1} + n_{\beta_2}) S_{\beta_1}. \tag{4.22}$$

Note that the winding numbers are introduced as $n_L := n_{\alpha_1} + n_{\alpha_2} - 2n_C$ and $n_C := n^{(+\infty)} - n^{(-\infty)}$.

The principle to incorporate the Stokes phenomenon is the same as before. The imaginary part

of complex paths is written as

$$\mathrm{Im}\, S_\Gamma = \mathrm{Im}\, S_{\Gamma_0} + (n_{\beta_1} + n_{\beta_2})\mathrm{Im}\, S_{\beta_1}, \tag{4.23}$$

and we require that the imaginary component of time t is decreasing. Under this condition, the complex path with the minimal imaginary action is given as the one with $n_{\beta_1} = n_{\beta_2} = 0$. The corresponding orbit starts from the left-side well and crosses over two potential barriers and reaches the right-side well. The resulting imaginary action is evaluated twice as much as the instanton action in each barrier:

$$\mathrm{Im}\, S_\Gamma = \mathrm{Im}\, S_{\beta_1}. \tag{4.24}$$

Concerning the real part of the action integral, the path Γ has to go half round the central well, so the real part of the action is given as

$$\mathrm{Re}\, S_\Gamma = n_L S_L + (n_C + \frac{1}{2})S_C, \tag{4.25}$$

and the Maslov index is also evaluated similarly to give $\mu = 2n_L + 2n_C + 3$. We finally get the semiclassical expression for the tunnelling splitting:

$$\Delta E_n \sim \frac{\hbar}{2T} e^{-S_{\beta_1}/\hbar} \sum_{n_L, n_C} (-1)^{\mu+1} e^{\mathrm{i}(n_L S_L + (n_C + \frac{1}{2})S_C)/\hbar}. \tag{4.26}$$

This almost coincides with the formula derived in [35] (see also equation (2.15)), but the way of enumerating the paths differs from the one adopted there, so the form of the sum is slightly different. As also discussed in [35], the interference caused by the sum in the right-hand side gives rise to resonances, which generate a series of spikes in the ΔE vs $1/\hbar$-plot. Such a phenomenon could be understood as the resonant tunnelling or the Fabry-Pérot effect in optics [36, 57].

4.3 Simultaneous quantization

As given in (4.8) and (4.21) the action integrals for the α loops in the fundamental group are related through the action integral associated with the loop encircling infinity. These relations will invoke *simultaneous quantization* of distinct wells. Simultaneous quantization in distinct wells has been discussed in Ref. [58], and the result obtained above is essentially the same as the one derived there in the double-well potential case.

We first explain how simultaneous quantization is achieved in the double-well case. Suppose the action integral for the left-side well is quantized as $S_L = (1/2 + m_L)2\pi\hbar$. From the relation (4.8), the action for the right well is also quantized as $S_R = (1/2 + m_R)2\pi\hbar$ if and only if the action integral around infinity satisfies the condition $S^{(\infty)} = 2\pi\hbar m^{(\infty)}$, where m_R, m_L and $m^{(\infty)}$ are integers.

Concerning the triple-well system, the relation (4.21) among action integrals is not enough to give simultaneously quantization of S_L and S_R even if $S^{(\infty)} = 2\pi\hbar m^{(\infty)}$ with integers $m^{(\infty)}$ is satisfied. However, if the potential is symmetric as assumed in section 4.2, S_L and S_R are quantized simultaneously since $S_L = S_R$ follows in such a case.

Note that the relations (4.8) and (4.21) hold among the α loops in the fundamental group. It would be natural to explore whether or not the relation involving β loops exist, which might provide further constraints for action integrals. Integrals of algebraic functions along α or β loops are called periods of Abelian integrals [55]. In a general argument of Abelian integrals, the period of Abelian integrals of the first kind has a relation as

$$\left(\int_{\beta_1}\omega, \cdots, \int_{\beta_g}\omega\right) = \left(\int_{\alpha_1}\omega, \cdots, \int_{\alpha_g}\omega\right) T, \tag{4.27}$$

where T is called the period matrix and ω is the Abelian differential of the first kind, respectively [59]. However, since the function $p(q)$ has poles in the Riemann surface, the relation among α or β loops might not take a linear form as given in (4.27). If the relation is linear, it would not provide an additional relation generating extra constraints concerning the quantization condition.

4.4 Normal form Hamiltonian system

In this section, we examine the case where the Hamiltonian is built from more general normal forms and whose tunnelling splittings were semiclassically studied in Ref. [43] in order to investigate the validity of the so-called RAT scenario [6, 7]. As shown below, equi-energy contours look like typical patterns observed in the Poincaré section of phase space in two-dimensional nearly-integrable systems. In the following we consider a Hamiltonian of the form [10]

$$H(p,q) = \sum_{k=1}^{n} a_k (p^2+q^2)^k + \sum_{l,m} b_{l,m} q^l p^m, \tag{4.28}$$

where a_k and $b_{l,m}$ are constants. Note that the b's are not all independent and depend only on the 2 real parameters. The argument based on the fundamental group for algebraic functions holds, in particular, the formula (3.7) for the path Γ.

As shown in an example below, if the coefficient of the highest order of p in the Hamiltonian does not depend on the variable q, the action integral along γ_i loop turns out to be 0 (see Appendix C).

More specifically we will work with

$$H(p,q) = \frac{1}{2}(p^2+x^2) - \frac{1}{2}(p^2+x^2)^2 - 2x^2p^2, \tag{4.29}$$

where $x := 1-q^2$. The symmetry condition (3.1) is maintained. As seen in the phase space portrait drawn in figure 4.10, the system has two symmetric wells located at the positions $q = \pm 1$ respectively, and nonlinear resonance like equi-energy contours appear around each well.

In order to perform semiclassical analysis for the tunnelling splitting, as was done in the previous examples, we first examine the Riemann surface and the associated fundamental group. From the Hamiltoninan (4.29), we easily find

$$p(q) = \sqrt{\pm\frac{\sqrt{-8E+32x^4-8x^2+1}}{-2} - 3x^2 + \frac{1}{2}}. \tag{4.30}$$

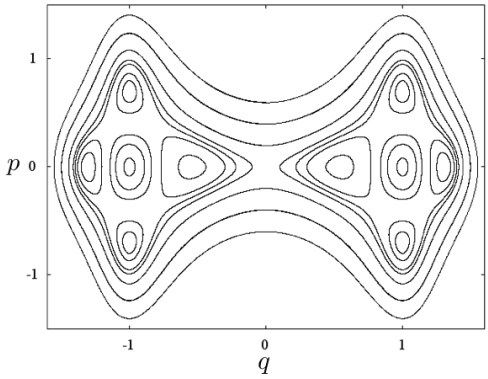

Figure 4.10: Equi-energy contours for the Hamiltonian (4.29).

The branch points are obtained by solving simultaneous algebraic equations

$$\pm\frac{\sqrt{-8E+32x^4-8x^2+1}}{-2}-3x^2+\frac{1}{2}=0,$$
$$-8E+32x^4-8x^2+1=0,$$

which provide 24 branch points in total. Each branch point is locally square-root type, thereby the corresponding Riemann surface R has four leaves. Using the formula evaluating the genus, we find that the Riemann surface R is homeomorphic to 9-fold torus with 28 small holes associated with 4 poles and 24 branch points. The Riemann surface is illustrated in figure 4.11. There are 9 α- and β-loops together with 24 γ-loops associated with the branch points and 4 γ-loops with poles, each of which is attached in the corresponding leaf. From these observations, we have 45 independent action integrals in the semiclassical formula. However, as shown in Appendix C, the action integrals for γ-loops for branch points are all zero, and the residues at the poles vanish. This fact simplifies the expression of action integrals as

$$S_\Gamma = S_{\Gamma_0}+\sum_{i=1}^{9} n_{\alpha_i}S_{\alpha_i}+\sum_{i=1}^{9} n_{\beta_i}S_{\beta_i}. \tag{4.31}$$

The next step is to single out the most dominant path out of all the candidates given above. Since $dq = pdt$ does not hold any more, we cannot a priori compare the different $\mathrm{Im}\, S$ even with

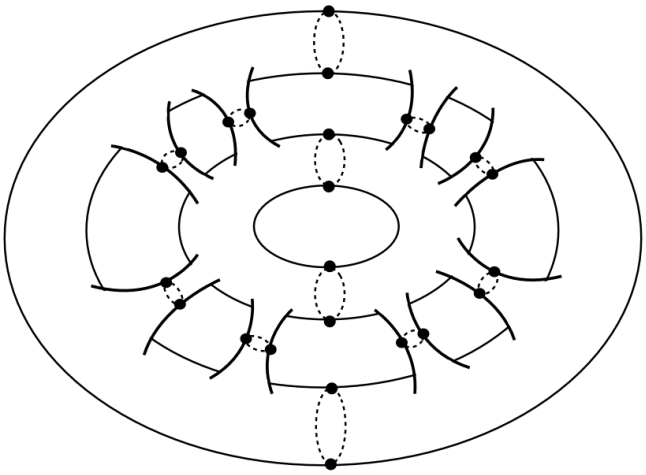

Figure 4.11: The Riemann surface of $p(q)$ for the Hamiltonian (4.29). The Riemann surface forms a 9-fold torus. The black dots and dashed curves are branch points and branch cuts, respectively.

an increasing $\mathrm{Im}\, dt < 0$ and the usual heuristic selection argument may fail, as will be shown below.

4.5 Tunnelling splitting for the normal form Hamiltonian system

In the following, we discuss the tunnelling splitting ΔE_n for the normal form Hamiltonian (4.29) based on the semiclassical analysis. Note however that the semiclassical analysis performed here will not fully be based on the semiclassical formula (3.3), and could be done only with a heuristic recipe. This is because, as shown below, that non-trivial situations actually arise from the handling of the Stokes phenomenon, so the selection of the most dominant complex path would be highly non-trivial. We focus on the tunnelling splitting $\Delta E_n = E_n^- - E_n^+$ for $E_n^+ \simeq E_n^- \simeq E$ below the barrier. Figure 4.12 plots ΔE_n as a function of $1/\hbar$ for $E = 6.19 \times 10^{-3}$.

In classical phase space, there appear congruent energy contour pairs in both sides of equi-energy contours, reflecting the symmetry with respect to the q-direction. For the energy satisfying $E \sim E_n^{\pm}$, there appear two closed energy contours in each side, which are shown in magenta

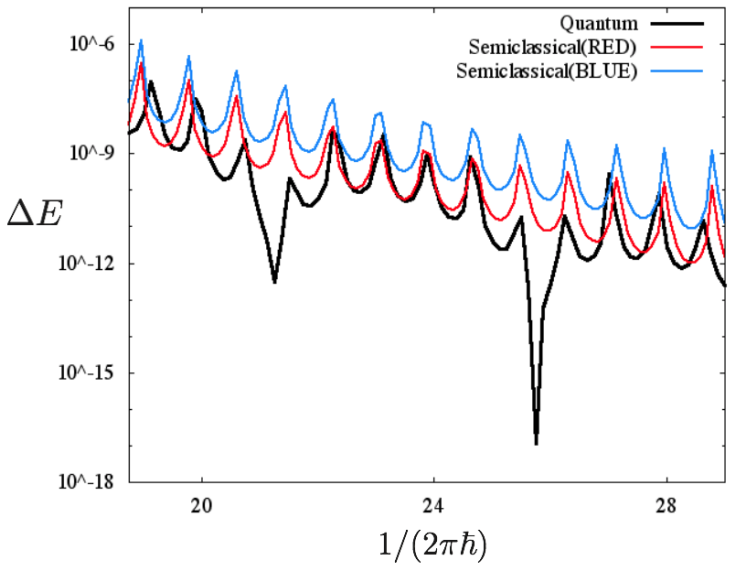

Figure 4.12: The tunnelling splitting $\Delta E_n = E_n^- - E_n^+$ as a function of $1/(2\pi\hbar)$. Here $E_n^+ \simeq E_n^- \simeq E = 6.19 \times 10^{-3}$. The black curve shows the numerical result obtained by direct calculation. The blue and red ones are obtained by applying the semiclassical formula (4.37), and the corresponding time paths are respectively shown in figure 4.15.

curves in figure 4.13. Obviously, due to the symmetry, there are only two characteristic real periods $T_{\rm out}$ and $T_{\rm in}$ and two actions $S_{\rm out}$ and $S_{\rm in}$ associated with the outer and inner orbits respectively. The latter are connected via complex manifolds, which are shown in blue curves in figure 4.13, and outer periodic orbits in both sides are also connected via complex manifolds, drawn in green curves. Complex manifolds are obtained by integrating Hamiltonian equations of motion in the purely imaginary direction starting from each point of periodic orbits.

Following the argument developed in Ref. [35], we consider the time path in the complex plane for the orbit contributing to the semiclassical formula (3.3). The total elapsed time T is written as

$$T \sim R(T) + {\rm i}T_{\rm in-out} + {\rm i}T_{\rm out-out} + {\rm i}T_{\rm in-out} + L(T), \tag{4.32}$$

where ${\rm i}T_{\rm in-out}$ is the time interval during which the complex orbit runs from the inner energy to the outer energy curve within the same well, shown in blue curves in figure 4.13. Similarly, ${\rm i}T_{\rm out-out}$ is the purely imaginary interval between the outer energy curve in the left side to another outer curve in the right side, shown in green curves in figure 4.13. $L(T)$ and $R(T)$ are sums of time intervals

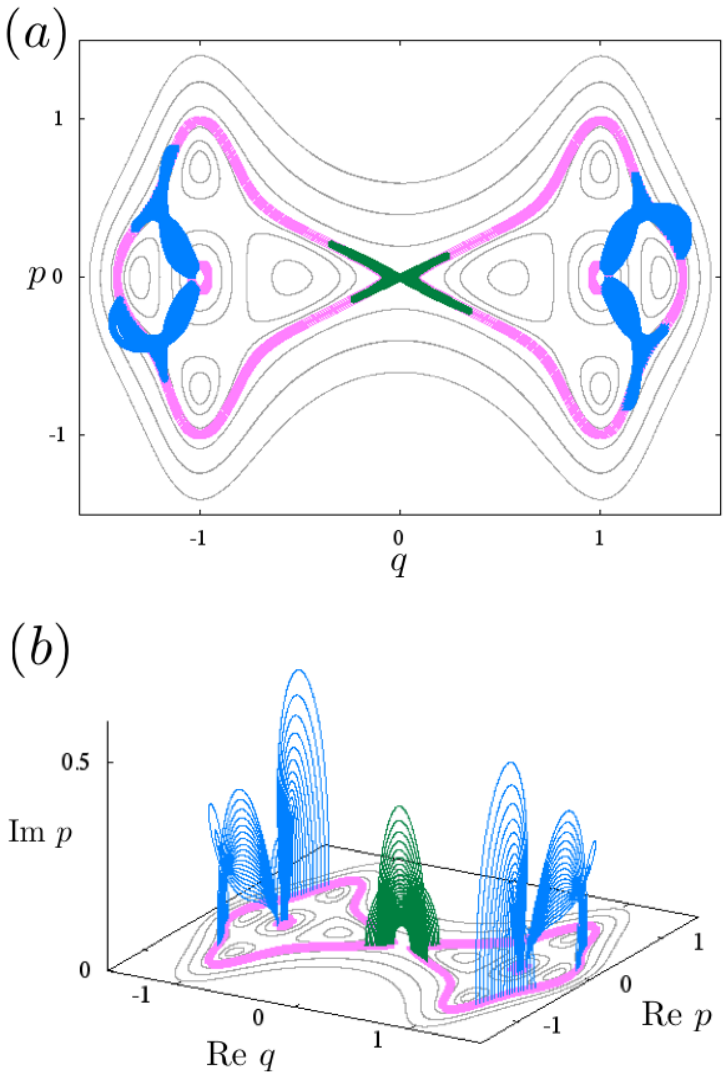

Figure 4.13: (a) Equi-energy contours for the Hamiltonian (4.29). The magenta curves show energy contours satisfying the condition $E \sim E_n^{\pm}$ where $E = 6.19 \times 10^{-3}$. The blue curves are projections onto the real plane of complex manifolds connecting inside and outside energy contours. The green one shows projection of complex manifold connecting left and right outer energy contours. (b) The projection of each manifold onto $(\mathrm{Re}\, q, \mathrm{Re}\, p, \mathrm{Im}\, p)$ space.

spent by the orbit moving in the inner and outer real energy curves, i.e.,

$$L(T) = n_{\rm in}T_{\rm in} + n_{\rm out}T_{\rm out}, \tag{4.33}$$

$$R(T) = n'_{\rm in}T_{\rm in} + n'_{\rm out}T_{\rm out}, \tag{4.34}$$

where the winding numbers $n_{\rm in}, n_{\rm out}, n'_{\rm in}$ and $n'_{\rm out}$ are taken to be positive integers. A comment concerning $L(T)$ and $R(T)$ is in order. In Ref. [35], a fractional time interval τ, or a residual time, was introduced for the time interval along the real direction as $\mathrm{Re}\, T = L(T) + R(T) - \tau$ in order to adjust the time interval in such a way that initial and final points are located at desired positions. However this residual time τ does not play any roles after taking the limit $\mathrm{Re}\, T \to \infty$ [35]. The corresponding action integral is then written as

$$\begin{aligned} S \sim\ & n_{\rm in}S_{\rm in} + {\rm i}S_{\rm in-out}/2 + n_{\rm out}S_{\rm out} \\ +\ & {\rm i}S_{\rm out-out}/2 \\ +\ & n'_{\rm in}S_{\rm in} + {\rm i}S_{\rm in-out}/2 + n'_{\rm out}S_{\rm out}, \end{aligned} \tag{4.35}$$

Here we focus only on the trajectories running on the complex manifolds connecting the real energy curves only once, as illustrated in figure 4.14. Hence, under the restrictions given in (4.33)

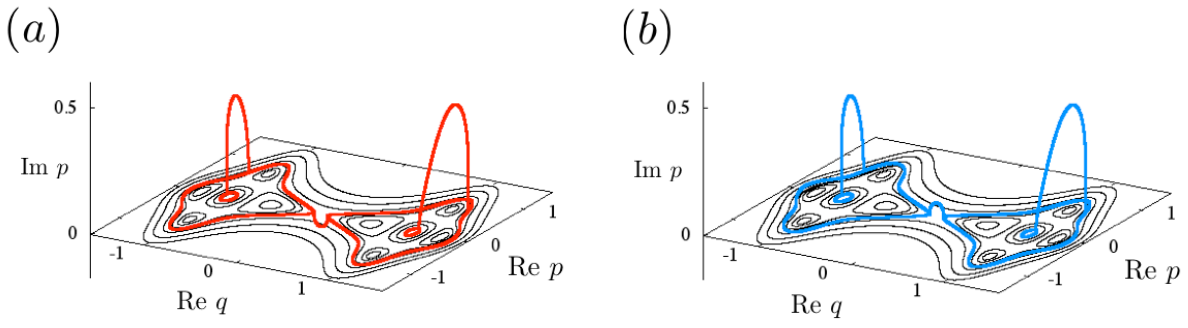

Figure 4.14: The projection of complex paths onto $(\mathrm{Re}\, q, \mathrm{Re}\, p, \mathrm{Im}\, p)$ space in the case (a) where the corresponding time path is taken as the red line in figure 4.15 and (b) where the blue path is taken, respectively. The energy for red and blue coloured curves is given as $E = 6.19 \times 10^{-3}$.

and (4.34), the sum of contributions of such trajectories takes the form as

$$\sum_{n_{\rm in}}\sum_{n'_{\rm in}}(-1)^{\mu+1}4(n_{\rm in}+1)4(n'_{\rm in}+1)e^{{\rm i}(n_{\rm in}S_{\rm in}+{\rm i}S_{\rm in-out}/2+n_{\rm out}S_{\rm out})/\hbar}$$
$$\times e^{(-S_{\rm out-out}/2)/\hbar}e^{{\rm i}(n'_{\rm in}S_{\rm in}+{\rm i}S_{\rm in-out}/2+n'_{\rm out}S_{\rm out})/\hbar}. \tag{4.36}$$

Here the Maslov index is evaluated as $\mu = n_{\rm in} + n_{\rm out} + n'_{\rm in} + n'_{\rm out} + 7$. We may take the sums for $n_{\rm in}$ and $n'_{\rm in}$ separably, and each sum is the same as the one in the triple-well case in Ref. [35]. These lead us to the semiclassical expression for the tunnelling splitting

$$\Delta E_n \sim \frac{2\hbar}{T_{\rm in}}\left(\frac{e^{-S_{\rm in-out}/(2\hbar)}}{\sin(((T_{\rm out}/T_{\rm in})S_{\rm in}-S_{\rm out})/(2\hbar))}\right)^2 e^{-S_{\rm out-out}/2\hbar}. \tag{4.37}$$

Using this formula, we now demonstrate that a proper treatment of the Stokes phenomenon is crucial to discuss the tunnelling splitting of the normal form Hamiltonian within the semiclassical framework. In figure 4.12, we compare the splitting calculated using direct diagonalization with the ones obtained using the semiclassical formula (4.37). In the semiclassical calculation, we show the splittings evaluated using the complex path, which are drawn as red and blue zig-zag lines in the complex time plane (see figure 4.15). Note that both paths connect the left- and right wells and satisfy the boundary conditions necessary for the semiclassical formula.

As noticed from figure 4.15, the time path shown in blue satisfies the condition that $\mathrm{Im}\,T$ monotonically decreases whereas the path in red breaks the monotonicity. According to the criterion adopted in sections 4.1 and 4.2, the red-coloured path should be dropped from the final contribution because the path contains an interval in which $\mathrm{Im}\,T$ increases and expected to provide an exponentially exploding contribution which should be excluded from the final sum. However, as seen in figure 4.12, the curve based on the red-path contribution gives a larger slope as compared to the blue one, and shows better fitting to the exact plot. This result provides evidence implying that a naive criterion to treat the Stokes phenomenon does not work in the case studied here. The result also strongly suggests that exponentially decreasing solutions do not necessarily remain as contributions. This is counterintuitive in the conventional semiclassical argument as well.

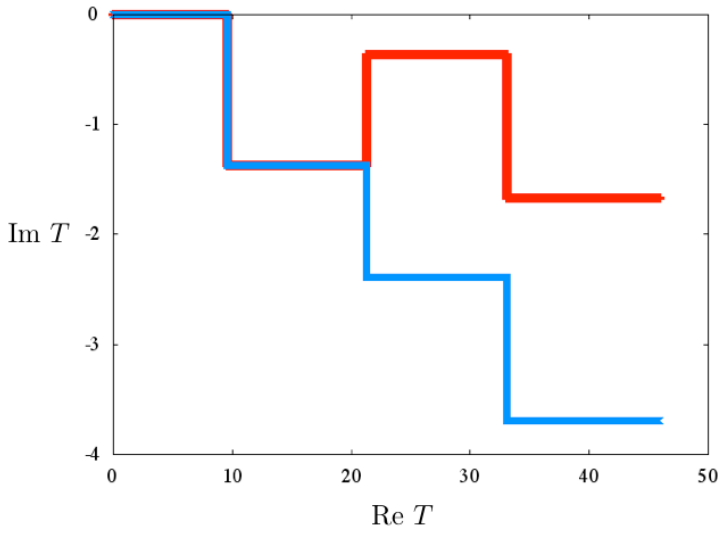

Figure 4.15: Complex time paths which are taken to test the semiclassical formula (see text). The imaginary time monotonically decreases in the blue path case while monotonicity condition is not satisfied in the red path case.

Chapter 5

Summary and discussion

In this thesis, we have discussed tunnelling splittings based on semiclassical analysis, and investigated the topology of complex paths in 1-dimensional systems to enumerate possible complex paths which contribute to the semiclassical sum formula for tunnelling splittings. One of our main claims is, as compared conventional complex trajectory based approaches to tunnelling splittings, that it would not be a reasonable strategy to explore the complex paths as a function of time t, instead one should examine the complex path on the configuration space because infinitely many singularities and as a result infinitely many topologically distinct paths inevitably appear in the complex time plane even in simple systems. Here Hamiltonian functions were assumed to be written as polynomials of the variables p and q, thereby we could make use of knowledge on algebraic functions, especially the fundamental group for the Riemann surface. Since the action integral is the most important ingredient in the semiclassical formula, we examined the Riemann surface of the function $p(q)$ closely and showed that it has a finite number of leaves and homeomorphic to a multi-handled compact surface. The number of loops of the homology basis for the associated fundamental group turns out to be finite, reflecting the fact that the function $p(q)$ is algebraic.

To enumerate independent action integrals, it would be natural to consider independent elements in the fundamental group of the function $p(q)$. However this is not enough for our semiclassical analysis because the action integral is defined by the integration of $p(q)$ along an integration contour, so one has to take into account not only branch points generating the multivaluedness of the function $p(q)$, but also other singularities of $p(q)$ with non-zero residues. Such singularities

indeed appear in the Riemann surface as divergent points of $p(q)$.

As model systems, we here studied the double- and triple-well potential systems, together with the normal form Hamiltonians as well. For the former two cases, we have obtained the complete list of the possible complex paths based on the idea employing the fundamental group. As a bi-product out of such a systematic treatment, we derived action relations involving the residue contribution from divergent points of $p(q)$. Note that the relation for the double-well case has already been obtained in [58], but its origin could more simply be understood through the fundamental group argument. In the case of the double-well potential system for instance, we usually consider the quantization condition for each well independently since the equi-energy surfaces in left- and right-side wells are classically disjoined. However our analysis exploring the topology of the whole complex equi-energy surfaces has unveiled that quantization conditions in left- and right-wells are linked through the action integral associated with infinity of the Riemann surface. Similar action relations were similarly derived in the triple-well potential system, and they lead to simultaneous quantization of left- and right-wells if the potential is symmetric.

In performing the semiclassical analysis, it is not sufficient to enumerate the complex paths satisfying the boundary conditions required in the semiclassical formula. Since the semiclassical formula is obtained by applying the saddle point method, one needs to handle the Stokes phenomenon in an appropriate manner. In the semiclassical arguments for tunnelling splittings so far, this issue has not been discussed seriously even in 1-dimensional situations. The most typical approach would be just to remove exponentially exploding solutions, which is based only on a rather naive speculation in analogy with a treatment of the Airy function. The well-known instanton theory and its variants applied to more general situations have adopted essentially the same strategy. However, as shown in the present thesis, the possible classical actions are expressed as a linear combination of elements of the fundamental group together with contributions from divergent singularities. This brings infinitely many possible candidates, and infinitely many exploding solutions are necessarily contained among them. As a result, it becomes a crucial step to deal with the Stokes phenomenon properly. This is entirely beyond the scope of this thesis, and here we only tested the most conventional prescription. For the double- and triple-well potential systems, we extracted the complex paths remaining as semiclassical contributions in such a way that the imaginary direction

of the corresponding time path should be negative, which guarantees the monotonicity of imaginary action of complex paths. We confirmed that the results were both consistent with known results.

In the normal form Hamiltonian case, we could also find all the possible complex paths based on the fundamental group because the Hamiltonian is also given as a polynomial function. However, a naive treatment of the Stokes phenomenon was shown to break down. In particular, we demonstrated that there is a situation where even exponentially decaying contributions should be dropped, which is one piece of evidence suggesting that the Stokes phenomenon for the normal form Hamiltonian systems must be highly non-trivial [60].

Our motivation for studying the normal form Hamiltonian was to promote our understanding of the so-called resonance-assisted tunnelling as was done in [43]. As stressed in this thesis, equi-energy contours of the normal form Hamiltonian apparently look like patterns typically appearing in Poincaré sections of two-dimensional nearly integrable system, but nonlinear resonance like structures in 1-dimensional systems are not caused by nonlinear resonances. It would therefore be unreasonable to explain the mechanism of tunnelling occurring in two-dimensional nonintegrable systems based on 1-dimensional systems even though apparent similarity exists in their phase space patterns.

Even if one concedes that the normal form Hamiltonian could somehow serve as an analogous model to the system with nonlinear resonances, the analysis based on the fundamental group tells us that what is relevant is the topology of the Riemann surface, which is entirely controlled by the branch points of the function $p(q)$. This implies that instanton in the conventional sense might play only a relative role. The understanding of instanton has been updated from the perspective of the relevance of the Riemann sheet structure, which is based on a similar spirit as our present arguments [61, 62].

One important message out of this thesis would be that one does not need to consider the time path any more and has only to focus on the function $p(q)$. Instanton has a long history and the idea using the complex time plane has been and still might be predominant, but we believe that this would not be a right strategy as discussed in the present thesis and Refs. [61, 62] as well. What we need is information on the function $p(q)$, not the complex structure of functions $q(t)$ and $p(t)$, so

analyzing the fundamental group for the Riemann surface of $p(q)$ would become unavoidable.

Appendix A

Exact solution of equations of motion

A.1 Exact solution in triple-well potential system

Let us consider a Hamiltonian,

$$H = \frac{p^2}{2} + V(q), \tag{A.1}$$

where the potential is given as

$$V(q) = (q^2 - a^2)^2(q^2 - b^2). \tag{A.2}$$

In what follows we will provide the exact solution for the Hamiltonian equation for this system.

From the energy conservation law,

$$E = \frac{p^2}{2} + V(q), \tag{A.3}$$

we obtain,

$$\int dt = \int \frac{dq}{\sqrt{2(E - V(q))}}. \tag{A.4}$$

In case of (A.2), the right hand side is expressed as

$$\int \frac{dq}{\sqrt{2(E-(q^2-a^2)^2(q^2-b^2))}}. \tag{A.5}$$

Introducing the coordinate transformation $x = q^2 - a^2$, the above integral is rewritten as

$$\int \frac{dx}{2\sqrt{2(x+a^2)\left(E-x^2(x+a^2-b^2)\right)}}. \tag{A.6}$$

Then we write it in the form as

$$\int \frac{dx}{2\sqrt{-2(x-\alpha)(x-\beta)(x-\gamma)(x-\delta)}}, \tag{A.7}$$

the constants $\alpha, \beta, \gamma, \delta$ are solutions for the 4th order algebraic equation, which is given by setting the denominator of equation (A.6) to be zero [1]. Furthermore, we convert the coordinate as

$$y^2 = \frac{(\beta-\delta)(x-\alpha)}{(\alpha-\delta)(x-\beta)} \tag{A.8}$$

$$k^2 = \frac{(\beta-\gamma)(\alpha-\delta)}{(\alpha-\gamma)(\beta-\delta)} \tag{A.9}$$

$$M^2 = \frac{(\beta-\delta)(\alpha-\gamma)}{4}, \tag{A.10}$$

then we obtain

$$\int \frac{dx}{2\sqrt{-2(x-\alpha)(x-\beta)(x-\gamma)(x-\delta)}} = \frac{1}{2\sqrt{-2}} \int \frac{dy}{M\sqrt{(1-y^2)(1-k^2y^2)}}. \tag{A.11}$$

Since the right side of equation (A.11) is just an elliptic integral [63–65], one solution for the equation (A.5) is written using the Jacobi elliptic function sn as,

$$q_{\mathrm{sn}}(t) = \sqrt{\frac{-(\beta-\delta)(a^2+\alpha)+(\alpha-\delta)(a^2+\beta)\mathrm{sn}^2(2\sqrt{-2}Mt,k)}{(\alpha-\delta)\mathrm{sn}^2(2\sqrt{-2}Mt,k)-(\beta-\delta)}}. \tag{A.12}$$

[1] These are controlled by E, a, and b.

Another one is given using the Jacobi elliptic functions cn,

$$q_{\mathrm{cn}}(t) = \sqrt{\frac{(a^2+\delta)(\alpha-\beta)-(\alpha-\delta)(a^2+\beta)\mathrm{cn}^2(-2\sqrt{-2}Mt,k)}{(\alpha-\beta)-(\alpha-\delta)\mathrm{cn}^2(-2\sqrt{-2}Mt,k)}}. \tag{A.13}$$

Singularities (divergence points) of these solutions on the complex time plane are given by the condition

$$\sqrt{\frac{-(\beta-\delta)(a^2+\alpha)+(\alpha-\delta)(a^2+\beta)\mathrm{sn}^2(2\sqrt{-2}Mt,k)}{(\alpha-\delta)\mathrm{sn}^2(2\sqrt{-2}Mt,k)-(\beta-\delta)}} = \pm\infty, \tag{A.14}$$

which leads to an implicit condition

$$\mathrm{sn}^2(2\sqrt{-2}Mt,k) = \frac{\beta-\delta}{\alpha-\delta}. \tag{A.15}$$

We can extend the method described here to more general cases. One generalization would be to take $V(q) = (q^2-a^2)(q^2-b^2)(q^2-c^2)$. In this case, we can solve the equations of motion in the same manner by introducing $x = q^2 - a^2$. More general variable transformation such as $g(x) = f(q)$, where both $g(x)$ and $f(q)$ are polynomial functions of x and q respectively allows us to provide exact solutions for higher order potential systems.

A.2 Exact solution in n-th order normal form Hamiltonian systems

In this section, we show the exact solution of Hamilton equation for the one-dimensional n-th order normal form Hamiltonian. We recall the definition of the normal form Hamiltonian:

$$H = \sum_{k=1}^{n} a_k(p^2+q^2)^k + \sum_{l,m} b_{l,m}q^l p^m, \tag{A.16}$$

which is introduced in [10]. In the (p,q)-phase space, the phase space exhibits resonance-like chain structure (See figure 4.10). A classification of generic bifurcation of the phase space structure was

first studied in [66], and further examined in [67]. Semiclassically, the analysis of the energy spectrum according to the periodic-orbit sum formula was studied in [68].

Let us introduce new variables as

$$P := p^2, \tag{A.17}$$

$$Q := q^2. \tag{A.18}$$

Using these variables, we consider the following Hamiltonian

$$H = \sum_{k=1}^{n} a_k (Q+P)^k + f(Q,P;l,m), \tag{A.19}$$

where

$$f(Q,P;l,m) = \sum_{l,m} b_{l,m} Q^{l/2} P^{m/2} \tag{A.20}$$

represents the resonance terms. The derivative of P, Q with respect to time t gives

$$\dot{Q} = 2q\dot{q} = 2q\frac{\partial H}{\partial p} = \sum_k k a_k (Q+P)^{k-1}(4\sqrt{QP}) + 2\sqrt{Q} f_p, \tag{A.21}$$

$$\dot{P} = 2p\dot{p} = 2p\frac{-\partial H}{\partial q} = -\sum_k k a_k (Q+P)^{k-1}(4\sqrt{QP}) - 2\sqrt{P} f_q, \tag{A.22}$$

where prime $\dot{}$ denotes the derivative with respect to time t and f_q, f_p are the partial derivative of f with respect to the variables q and p, respectively. Then we get

$$\dot{Q} + \dot{P} = 2\sqrt{Q} f_p - 2\sqrt{P} f_q, \tag{A.23}$$

$$\dot{Q} - \dot{P} = 2\sum_k k a_k (Q+P)^{k-1}(4\sqrt{QP}) + 2\sqrt{Q} f_p + 2\sqrt{P} f_q. \tag{A.24}$$

Here, the right-hand side of equation (A.23) and equation (A.24) are

$$\begin{aligned}
& 2\sqrt{Q}f_p + 2\sqrt{P}f_q \\
= & \sum_{l,m} \frac{m}{2} b_{l,m} Q^{\frac{l}{2}} P^{\frac{m}{2}-1} (4\sqrt{QP}) + \sum_{l,m} \frac{l}{2} b_{l,m} Q^{\frac{l}{2}-1} P^{\frac{m}{2}} (4\sqrt{QP}) \\
= & \sum_{l,m} \frac{m}{2} b_{l,m} Q^{\frac{l}{2}} P^{\frac{m}{2}-1} (4\sqrt{QP}) + \sum_{l,m} (\frac{l}{2} - \frac{m}{2}) b_{l,m} Q^{\frac{l}{2}-1} P^{\frac{m}{2}} (4\sqrt{QP}) \\
& + \sum_{l,m} \frac{m}{2} b_{l,m} Q^{\frac{l}{2}-1} P^{\frac{m}{2}} (4\sqrt{QP}) \\
= & (Q+P) \sum_{l,m} \frac{m}{2} b_{l,m} Q^{\frac{l}{2}-1} P^{\frac{m}{2}-1} (4\sqrt{QP}) + \sum_{l,m} (\frac{l}{2} - \frac{m}{2}) b_{l,m} Q^{\frac{l}{2}-1} P^{\frac{m}{2}} (4\sqrt{QP}),
\end{aligned} \tag{A.25}$$

$$\begin{aligned}
& 2\sqrt{Q}f_p - 2\sqrt{P}f_q \\
= & \sum_{l,m} \frac{m}{2} b_{l,m} Q^{\frac{l}{2}} P^{\frac{m}{2}-1} (4\sqrt{QP}) - \sum_{l,m} \frac{l}{2} b_{l,m} Q^{\frac{l}{2}-1} P^{\frac{m}{2}} (4\sqrt{QP}) \\
= & \sum_{l,m} \frac{m}{2} b_{l,m} Q^{\frac{l}{2}} P^{\frac{m}{2}-1} (4\sqrt{QP}) - \sum_{l,m} (\frac{l}{2} - \frac{m}{2}) b_{l,m} Q^{\frac{l}{2}-1} P^{\frac{m}{2}} (4\sqrt{QP}) \\
& - \sum_{l,m} \frac{m}{2} b_{l,m} Q^{\frac{l}{2}-1} P^{\frac{m}{2}} (4\sqrt{QP}) \\
= & (Q-P) \sum_{l,m} \frac{m}{2} b_{l,m} Q^{\frac{l}{2}-1} P^{\frac{m}{2}-1} (4\sqrt{QP}) - \sum_{l,m} (\frac{l}{2} - \frac{m}{2}) b_{l,m} Q^{\frac{l}{2}-1} P^{\frac{m}{2}} (4\sqrt{QP}).
\end{aligned} \tag{A.26}$$

Then we obtain

$$\begin{aligned}
\dot{Q} + \dot{P} &= (Q-P) \sum_{l,m} \frac{m}{2} b_{l,m} Q^{\frac{l}{2}-1} P^{\frac{m}{2}-1} (4\sqrt{QP}) - \sum_{l,m} (\frac{l}{2} - \frac{m}{2}) b_{l,m} Q^{\frac{l}{2}-1} P^{\frac{m}{2}} (4\sqrt{QP}), \\
\dot{Q} - \dot{P} &= 2 \sum_k k a_k (Q+P)^{k-1} (4\sqrt{QP}) + (Q+P) \sum_{l,m} \frac{m}{2} b_{l,m} Q^{\frac{l}{2}-1} P^{\frac{m}{2}-1} (4\sqrt{QP}) \\
& \quad + \sum_{l,m} (\frac{l}{2} - \frac{m}{2}) b_{l,m} Q^{\frac{l}{2}-1} P^{\frac{m}{2}} (4\sqrt{QP}).
\end{aligned}$$

In order to cancel the sum: $\sum_{l,m} \frac{m}{2} b_{l,m} Q^{\frac{l}{2}-1} P^{\frac{m}{2}-1} (4\sqrt{QP})$, we rewrite the above relations as

$$\begin{aligned}
\dot{Q} + \dot{P} &+ \sum_{l,m} (\frac{l}{2} - \frac{m}{2}) b_{l,m} Q^{\frac{l}{2}-1} P^{\frac{m}{2}} (4\sqrt{QP}) \\
&= (Q-P) \sum_{l,m} \frac{m}{2} b_{l,m} Q^{\frac{l}{2}-1} P^{\frac{m}{2}-1} (4\sqrt{QP}), \\
\dot{Q} - \dot{P} &- 2 \sum_{k} k a_k (Q+P)^{k-1} (4\sqrt{QP}) - \sum_{l,m} (\frac{l}{2} - \frac{m}{2}) b_{l,m} Q^{\frac{l}{2}-1} P^{\frac{m}{2}} (4\sqrt{QP}) \\
&= (Q+P) \sum_{l,m} \frac{m}{2} b_{l,m} Q^{\frac{l}{2}-1} P^{\frac{m}{2}-1} (4\sqrt{QP}),
\end{aligned}$$

and take the ratio of both sides, which leads to

$$\frac{\dot{Q} + \dot{P} + \sum_{l,m} (\frac{l}{2} - \frac{m}{2}) b_{l,m} Q^{\frac{l}{2}-1} P^{\frac{m}{2}} (4\sqrt{QP})}{\dot{Q} - \dot{P} - 2\sum_k k a_k (Q+P)^{k-1} (4\sqrt{QP}) - \sum_{l,m} (\frac{l}{2} - \frac{m}{2}) b_{l,m} Q^{\frac{l}{2}-1} P^{\frac{m}{2}} (4\sqrt{QP})} = \frac{(Q-P)}{(Q+P)}.$$

This gives the relation

$$\begin{aligned}
&(Q+P) \left\{ \dot{Q} + \dot{P} + \sum_{l,m} (\frac{l}{2} - \frac{m}{2}) b_{l,m} Q^{\frac{l}{2}-1} P^{\frac{m}{2}} (4\sqrt{QP}) \right\} = \\
&(Q-P) \left\{ \dot{Q} - \dot{P} - 2 \sum_{k} k a_k (Q+P)^{k-1} (4\sqrt{QP}) - \sum_{l,m} (\frac{l}{2} - \frac{m}{2}) b_{l,m} Q^{\frac{l}{2}-1} P^{\frac{m}{2}} (4\sqrt{QP}) \right\}.
\end{aligned}$$

Integrating both sides, we get

$$\begin{aligned}
\frac{1}{2}(Q+P)^2 - \frac{1}{2}(Q-P)^2 &= \int -2(Q-P) \sum_k k a_k (Q+P)^{k-1} (4\sqrt{QP}) \\
&- (Q-P) \sum_{l,m} (\frac{l}{2} - \frac{m}{2}) b_{l,m} Q^{\frac{l}{2}-1} P^{\frac{m}{2}} (4\sqrt{QP}) \\
&- (Q+P) \sum_{l,m} (\frac{l}{2} - \frac{m}{2}) b_{l,m} Q^{\frac{l}{2}-1} P^{\frac{m}{2}} (4\sqrt{QP}) dt.
\end{aligned} \tag{A.27}$$

In the following, we write the above relation in the following form

$$(Q+P)^2 - (Q-P)^2 = I(t), \tag{A.28}$$

by introducing

$$\begin{aligned} I(t) &:= \int -2(Q-P)\sum_k k a_k (Q+P)^{k-1}(4\sqrt{QP}) \\ &- (Q-P)\sum_{l,m}(\frac{l}{2}-\frac{m}{2})b_{l,m}Q^{\frac{l}{2}-1}P^{\frac{m}{2}}(4\sqrt{QP}) \\ &- (Q+P)\sum_{l,m}(\frac{l}{2}-\frac{m}{2})b_{l,m}Q^{\frac{l}{2}-1}P^{\frac{m}{2}}(4\sqrt{QP})dt. \end{aligned} \tag{A.29}$$

Then we immediately get

$$Q+P = I^{1/2}(t)\cosh(\theta(t)), \tag{A.30}$$

$$Q-P = I^{1/2}(t)\sinh(\theta(t)), \tag{A.31}$$

and

$$QP = \frac{I(t)}{4}. \tag{A.32}$$

Our last task is therefore to obtain the function $I(t)$. To do this, we use the energy conservation relation,

$$\begin{aligned} E &= \sum_k a_k (Q+P)^k + f(Q,P;l,m) \\ &= \sum_{k=1}^{n} a_k (I^{1/2}\cosh\theta)^k + \sum_{l,m} b_{l,m}\left(\frac{I^{1/2}(\cosh\theta+\sinh\theta)}{2}\right)^{l/2}\left(\frac{I^{1/2}(\cosh\theta-\sinh\theta)}{2}\right)^{m/2}. \end{aligned} \tag{A.33}$$

This is an algebraic equation for $I(t)$, so it would be possible to solve $I(t)$ and express it as a

function of θ. We finally have solutions for $Q(t)$ and $P(t)$ in terms of $\theta(t)$ as

$$Q = \frac{1}{2}(I^{1/2}(\theta(t))\cosh(\theta(t)) + I^{1/2}(\theta(t))\sinh(\theta(t))), \tag{A.34}$$

$$P = \frac{1}{2}(I^{1/2}(\theta(t))\cosh(\theta(t)) - I^{1/2}(\theta(t))\sinh(\theta(t))). \tag{A.35}$$

Therefore our task is reduced to solving a first-order differential equation for $\theta(t)$, implicitly expressed in the form of (A.23) (or (A.24)).

A.3 An example of normal form Hamiltonian systems

We here consider an example of 1-dimensional Hamiltonian normal form systems,

$$H = \frac{p^2}{2} + \frac{q^2}{2} + \epsilon\left(\frac{p^2}{2} + \frac{q^2}{2}\right)^2 + \eta p^2 q^2, \tag{A.36}$$

where ϵ and η are parameters controlling the structure of the phase space. There appears nonlinear resonance-like structure which looks like the two-dimensional nonlinear resonance islands in non-integrable systems. As shown in figure A.1, the phase space (with $\epsilon = \eta = -2$) exhibits a resonance-like island chain around a central elliptic fixed point. The Hamilton equations are

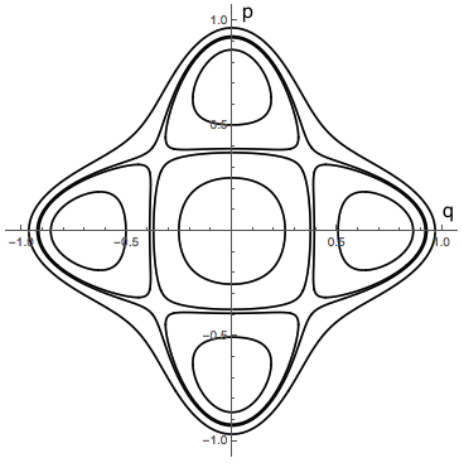

Figure A.1: The phase space for Hamiltonian (A.36) with $\epsilon = \eta = -2$.

written as

$$\dot{q} = p + \epsilon(q^2 p + p^3) + 2\eta p q^2, \tag{A.37}$$

$$\dot{p} = -q - \epsilon(q p^2 + q^3) - 2\eta p^2 q. \tag{A.38}$$

We define new variables

$$P := p^2, \tag{A.39}$$

$$Q := q^2, \tag{A.40}$$

then for $\dot{P}$ and $\dot{Q}$ we have

$$\dot{P} = 2p\dot{p}, \tag{A.41}$$

$$\dot{Q} = 2q\dot{q}. \tag{A.42}$$

The Hamilton equations are then rewritten as

$$\dot{Q} = (2 + 2\epsilon(Q + P) + 4\eta Q)\sqrt{PQ}, \tag{A.43}$$

$$\dot{P} = (-2 - 2\epsilon(P + Q) - 4\eta P)\sqrt{PQ}, \tag{A.44}$$

and we obtain

$$\dot{Q} + \dot{P} = 4\eta(Q - P)\sqrt{PQ}, \tag{A.45}$$

$$\dot{Q} - \dot{P} = (4 + 4\epsilon(P + Q) + 4\eta(P + Q))\sqrt{PQ}. \tag{A.46}$$

Combining these, we get

$$\frac{\dot{Q} + \dot{P}}{4\eta(Q - P)} = \sqrt{PQ} = \frac{\dot{Q} - \dot{P}}{4 + 4\epsilon(P + Q) + 4\eta(P + Q)}. \tag{A.47}$$

Multiplying equation (A.47) by $4\eta(Q-P)(4+4\epsilon(P+Q)+4\eta(P+Q))$, we have

$$\begin{aligned} 4(1+(\epsilon+\eta)(P+Q))(\dot{Q}+\dot{P}) &= 16\eta(Q-P)(1+(\epsilon+\eta)(P+Q))\sqrt{PQ} \\ &= 4\eta(Q-P)(\dot{Q}-\dot{P}). \end{aligned} \tag{A.48}$$

Both sides are integrated to get

$$\begin{aligned} 4(P+Q)+(2\epsilon+2\eta)(P+Q)^2 &= \int 4\eta(Q-P)(4+(4\epsilon+4\eta)(P+Q))\sqrt{PQ}dt \\ &= 2\eta(Q-P)^2+C, \end{aligned} \tag{A.49}$$

where C is a constant of integration. We here focus on the leftmost and rightmost sides in equation (A.49):

$$4(P+Q)+(2\epsilon+2\eta)(P+Q)^2 = 2\eta(Q-P)^2+C. \tag{A.50}$$

This can be regarded as an equation of a circle. After some calculations, we obtain

$$\frac{\eta(\epsilon+\eta)}{-1-(\epsilon+\eta)C}(Q-P)^2+\frac{-(\epsilon+\eta)^2}{-1-(\epsilon+\eta)C}\left\{(P+Q)+\frac{1}{\epsilon+\eta}\right\}^2=1. \tag{A.51}$$

Putting

$$\frac{-(\epsilon+\eta)^2}{-1-(\epsilon+\eta)C}\left\{(P+Q)+\frac{1}{\epsilon+\eta}\right\}^2=\sin^2\theta(t), \tag{A.52}$$

$$\frac{\eta(\epsilon+\eta)}{-1-(\epsilon+\eta)C}(Q-P)^2=\cos^2\theta(t), \tag{A.53}$$

where $\theta(t)$ is given through a differential equation for θ, which is discussed later. Then Q, P are

$$\begin{aligned} Q &= \frac{1}{2}\left((1+(\epsilon+\eta)C)^{1/2}\frac{1}{\epsilon+\eta}\sin\theta(t)-\frac{1}{\epsilon+\eta}+\left(\frac{1+(\epsilon+\eta)C}{-\eta(\epsilon+\eta)}\right)^{1/2}\cos\theta(t)\right), \\ P &= \frac{1}{2}\left((1+(\epsilon+\eta)C)^{1/2}\frac{1}{\epsilon+\eta}\sin\theta(t)-\frac{1}{\epsilon+\eta}-\left(\frac{1+(\epsilon+\eta)C}{-\eta(\epsilon+\eta)}\right)^{1/2}\cos\theta(t)\right). \end{aligned}$$

Putting $A := 1 + (\epsilon + \eta)C$, we finally reach the exact solution for the original variables q, p as

$$\begin{aligned} q &= \left(\frac{1}{2} \left(\frac{A^{1/2}}{\epsilon + \eta} \sin\theta(t) - \frac{1}{\epsilon + \eta} + \left(\frac{A}{-\eta(\epsilon + \eta)} \right)^{1/2} \cos\theta(t) \right) \right)^{1/2}, \\ p &= \left(\frac{1}{2} \left(\frac{A^{1/2}}{\epsilon + \eta} \sin\theta(t) - \frac{1}{\epsilon + \eta} - \left(\frac{A}{-\eta(\epsilon + \eta)} \right)^{1/2} \cos\theta(t) \right) \right)^{1/2}. \end{aligned} \tag{A.54}$$

C (or A) is a control parameter of the energy of trajectories.

A.3.1 Differential equation for $\theta(t)$

Our remaining task is to derive the equation for $\theta(t)$ and to solve it. Remember the left side equality in equation (A.47):

$$\frac{\dot{Q} + \dot{P}}{4\eta(Q - P)} = \sqrt{PQ}. \tag{A.55}$$

Here we express this equation in terms of $\theta(t)$, which provides a differential equation for $\theta(t)$. Since we already know expressions for Q and P as a function of $\theta(t)$, we have

$$\dot{Q} + \dot{P} = \frac{A^{1/2}}{\epsilon + \eta} \left(\dot{\theta}(t) \cos\theta(t) \right), \tag{A.56}$$

$$4\eta(Q - P) = 4\eta \left(\frac{A}{-\eta(\epsilon + \eta)} \right)^{1/2} \cos\theta(t), \tag{A.57}$$

and

$$QP = \frac{1}{4(\epsilon + \eta)^2} \left(A \sin\theta(t)^2 - 2A^{1/2} \sin\theta(t) + 1 + \frac{A(\epsilon + \eta)}{\eta} \cos\theta(t)^2 \right), \tag{A.58}$$

We insert these into equation (A.55) to obtain

$$\frac{\dot{\theta}(t)}{4\eta\left(\frac{\epsilon+\eta}{-\eta}\right)^{1/2}} = \sqrt{\frac{1}{4(\epsilon+\eta)^2}\left(A\sin^2(\theta(t)) - 2A^{1/2}\sin(\theta(t)) + 1 + \frac{A(\epsilon+\eta)}{\eta}\cos^2(\theta(t))\right)}. \tag{A.59}$$

This can be integrated as

$$\int \frac{dz}{\sqrt{1-\left(z+\frac{\eta}{A^{1/2}(-\epsilon)}\right)^2}\sqrt{\frac{1}{4(\epsilon+\eta)^2}\left(A\frac{-\epsilon}{\eta}z^2 + \frac{\eta}{\epsilon} + 1 + \frac{A(\epsilon+\eta)}{\eta}\right)}} = 4\left(-\eta(\epsilon+\eta)\right)^{1/2}\int dt,$$

where $z := \sin(\theta(t)) - \frac{\eta}{A^{1/2}(-\epsilon)}$. Introducing the notations for parameters as

$$\begin{aligned} z_\alpha &= -\frac{-\eta}{A^{1/2}\epsilon} + 1, \\ z_\beta &= -\frac{-\eta}{A^{1/2}\epsilon} - 1, \\ z_\gamma &= \sqrt{\frac{-\eta}{A\epsilon}(-\frac{\eta}{\epsilon} - 1 - \frac{A(\epsilon+\eta)}{\eta})}, \\ z_\delta &= -\sqrt{\frac{-\eta}{A\epsilon}(-\frac{\eta}{\epsilon} - 1 - \frac{A(\epsilon+\eta)}{\eta})}, \end{aligned} \tag{A.60}$$

the equation can be rewritten as

$$\int \frac{dz}{\sqrt{(z-z_\alpha)(z-z_\beta)(z-z_\gamma)(z-z_\delta)}} = \sqrt{\frac{4\epsilon A}{\epsilon+\eta}}\int dt. \tag{A.61}$$

Furthermore by setting

$$y^2 = \frac{(z_\beta - z_\delta)(z-z_\alpha)}{(z_\alpha - z_\delta)(z-z_\beta)}, \tag{A.62}$$

$$k^2 = \frac{(z_\beta - z_\gamma)(z_\alpha - z_\delta)}{(z_\alpha - z_\gamma)(z_\beta - z_\delta)}, \tag{A.63}$$

$$M^2 = \frac{(z_\beta - z_\delta)(z_\alpha - z_\gamma)}{4}, \tag{A.64}$$

the left-side hand can be expressed using the inverse function of the Jaboci elliptic sn function

$$\int \frac{dy}{\sqrt{M(1-y^2)(1-k^2y^2)}}. \tag{A.65}$$

We finally reach an explicit expression for $z(t)$ as

$$z(t) = \frac{-z_\alpha(z_\beta - z_\delta) + z_\beta(z_\alpha - z_\delta)\mathrm{sn}^2(\sqrt{\frac{4\epsilon A}{\epsilon+\eta}}Mt + t_0, k)}{(z_\alpha - z_\delta)\mathrm{sn}^2(\sqrt{\frac{4\epsilon A}{\epsilon+\eta}}Mt + t_0, k) - (z_\beta - z_\delta)}, \tag{A.66}$$

and for $\theta(t)$

$$\theta(t) = \arcsin(z(t) + \frac{-\eta}{A^{1/2}\epsilon}), \tag{A.67}$$

where t_0 is an initial condition of time.

A.3.2 Relation to the double-well system

In this section, we show a relation between $z(t)$ and the double-well potential system. Now recall the solution $z(t)$:

$$z(t) = \frac{-z_\alpha(z_\beta - z_\delta) + z_\beta(z_\alpha - z_\delta)\mathrm{sn}^2(\sqrt{\frac{4\epsilon A}{\epsilon+\eta}}Mt + t_0, k)}{(z_\alpha - z_\delta)\mathrm{sn}^2(\sqrt{\frac{4\epsilon A}{\epsilon+\eta}}Mt + t_0, k) - (z_\beta - z_\delta)}. \tag{A.68}$$

Note that the double-well potential system as four turning points, each of which is hereby denoted as $z(t) = z_\alpha, z_\beta, z_\gamma$, and z_δ. For simplicity, we set $t_0 = 0$ and $T = \sqrt{\frac{4\epsilon A}{\epsilon+\eta}}Mt$ in the following.

For $T = 0$, we have

$$z(0) = z_\alpha, \tag{A.69}$$

and for $T = K$,

$$z(K) = z_\delta, \tag{A.70}$$

which implies that z_α and z_δ form a pair. In the same way, for $T = \mathrm{i}K'$,

$$z(\mathrm{i}K') = z_\beta, \tag{A.71}$$

and for $T = K + \mathrm{i}K'$,

$$z(K + \mathrm{i}K') = z_\gamma. \tag{A.72}$$

This implies that the point z_β is connected with z_γ via a real torus and also we know that z_α and z_β are connected via a complex torus. K and K' are the real and imaginary period of the sn function, respectively. At each turning point, $z_\alpha, z_\beta, z_\gamma, z_\delta$, we have

$$\begin{aligned}
\theta(z_\alpha) &= \arcsin(z_\alpha + \frac{-\eta}{A^{1/2}\epsilon}) = \arcsin(1) = \frac{\pi}{2}, \\
\theta(z_\beta) &= \arcsin(z_\beta + \frac{-\eta}{A^{1/2}\epsilon}) = \arcsin(-1) = -\frac{\pi}{2}, \\
\theta(z_\gamma) &= \arcsin(z_\gamma + \frac{-\eta}{A^{1/2}\epsilon}) = \arcsin(\frac{\sqrt{(\epsilon+\eta)(A\epsilon+\eta)}}{A^{1/2}\epsilon}), \\
\theta(z_\delta) &= \arcsin(z_\delta + \frac{-\eta}{A^{1/2}\epsilon}) = \arcsin(-\frac{\sqrt{(\epsilon+\eta)(A\epsilon+\eta)}}{A^{1/2}\epsilon}).
\end{aligned}$$

For $z = z_\alpha$ and z_β, $q(t) = p(t)$ is satisfied, and $z = z_\gamma$, z_δ, $q(t) = 0$, or $p(t) = 0$ follows.

The correspondence between the double-well system and the phase space for the normal form Hamiltonian is shown in figure A.2. Since we fix the elliptic function's modular k as given in equation (A.63), the turning points of the double-well potential should be located as in figure A.2.

For comparison, we consider an orbit which starts from the point z_α in the double-well potential system (see the right top in figure A.2). Let t_α be time which is implicitly specified by the initial point z_α. Since $q(t_\alpha) = p(t_\alpha)$ holds, the corresponding position in phase space of the normal form Hamiltonian, denoted as "z_α", given as in figure A.2.

In the double-well system, the orbit described by $z(t)$ moves from z_α to z_δ along the real time axis and the period of oscillation z_α and z_δ is given as K. The orbit starting at "z_α" for the normal form Hamiltonian also moves to "z_δ", but the form of explicit solutions tell us that the sign of $q(t)$ and $p(t)$ changes its value either to -1 or 1, the orbit can move either $q(t) = 0$ or $p(t) = 0$ (notice

that there are two "z_δ" as shown in figure A.2). In other words, multivaluedness happens in case of the normal form Hamiltonian.

On the other hand, along the pure imaginary direction, the orbit starting at z_α moves to z_β during the period $\mathrm{i}K'$. This is nothing but the instanton orbit. In the normal form Hamiltonian, the orbit starting at "z_α" moves to "z_β" as shown in figure A.3.

In a similar way as the oscillation between "z_α" and "z_δ" along the real axis, the oscillation between "z_β" and "z_γ" with K happens in phase space of the normal form Hamiltonian.

Obviously the divergence points of $q(t)$ are found as the divergence points of $z(t)$, i.e., going along the imaginary time from z_δ or z_γ. Except for the singularities attaining zeros, there exist no further divergence points in this situation (See figure A.4).

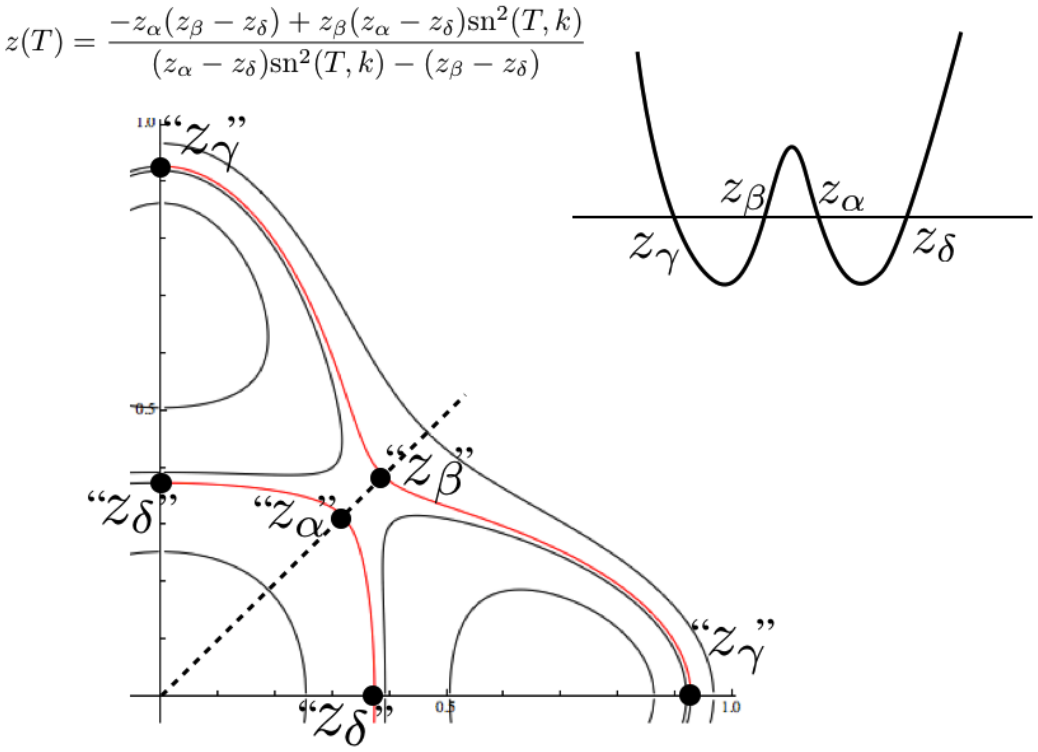

Figure A.2: The relation between the solution of the double-well potential and $z(t)$.The parameters are $\epsilon = -2, \eta = -2$.

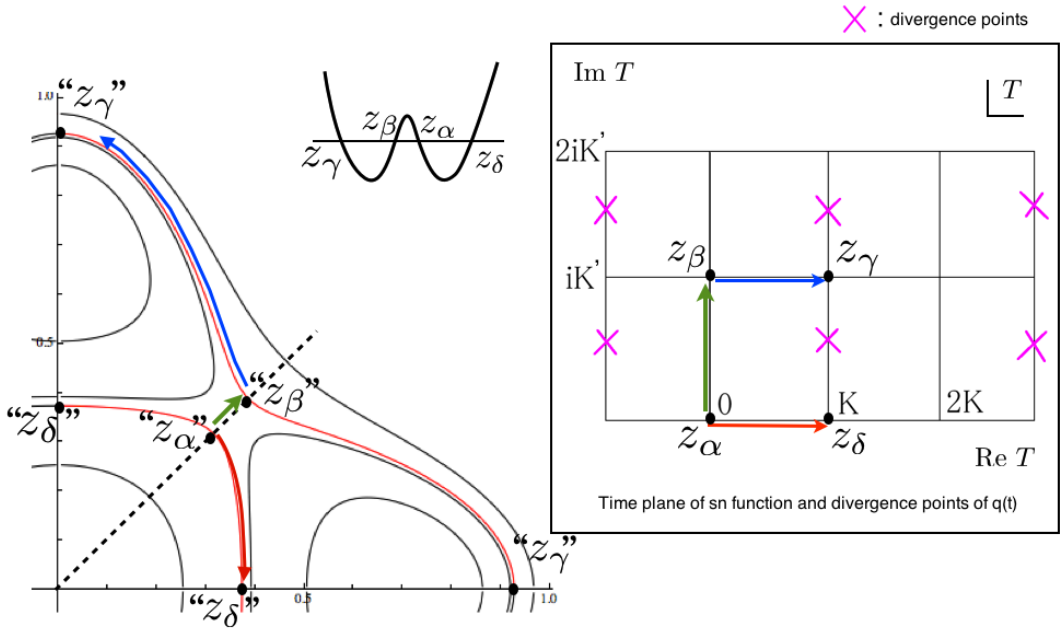

Figure A.3: A part of an orbit is put on the torus with $C = 0.12$. "z_α", "z_β", "z_γ", and "z_δ" are the positions of the orbit which are specified by z_α, z_β, z_γ, and z_δ in the double-well system, respectively. The red curve with arrow shows an orbit which moves from "z_α" to "z_δ" along the real time axis. The green curve shows an orbit which moves from "z_α" to "z_β" along the imaginary time axis. The blue curve shows an orbit which moves from "z_β" to "z_γ" along the real time axis. A sketch of the double-well potential with turning points is put on the top right.

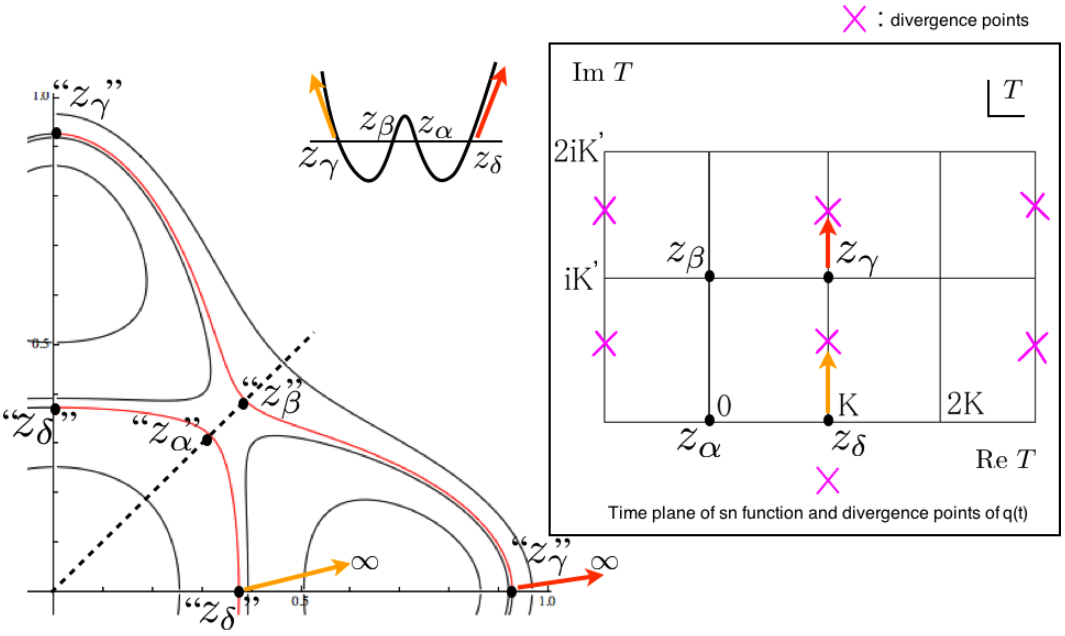

Figure A.4: Singularities (divergence points) of $q(t)$ on the complex time plane of sn function.

Appendix B

Semiclassical formula of tunnel splittings

In this appendix, we briefly sketch the derivation of the formula (3.3), following Ref. [35]. Let $|\phi_n^{\pm}\rangle$ be symmetric and asymmetric quasi-degenerated states for a Hamiltonian commuting with the parity operator $\hat{S}$ such that $\hat{S}^2 = 1$. The eigenstates of $\hat{H}$ can be classified according to their parity,

$$\hat{S}|\phi_n^{\pm}\rangle = \pm|\phi_n^{\pm}\rangle. \tag{B.1}$$

The spectral decomposition of the evolution operator after a time T writes

$$\hat{U}(T) = \sum_n (e^{\frac{1}{i\hbar}E_n^+ T}|\phi_n^+\rangle\langle\phi_n^+| + e^{\frac{1}{i\hbar}E_n^- T}|\phi_n^-\rangle\langle\phi_n^-|). \tag{B.2}$$

To discuss the tunnelling splitting between the states $|\phi_n^+\rangle$ and $|\phi_n^-\rangle$, we further define the projection operator

$$\hat{\Pi}_n = \phi_n^+\rangle\langle\phi_n^+| + |\phi_n^-\rangle\langle\phi_n^-|, \tag{B.3}$$

and we have

$$\mathrm{Tr}(\hat{\Pi}_n\hat{U}) = \sum_m \langle\phi_m^{\pm}|\hat{\Pi}_n\hat{U}|\phi_m^{\pm}\rangle = e^{-\frac{\mathrm{i}}{\hbar}E_n^+ T} + e^{-\frac{\mathrm{i}}{\hbar}E_n^- T}, \tag{B.4}$$

$$\mathrm{Tr}(\hat{S}\hat{\Pi}_n\hat{U}) = e^{-\frac{\mathrm{i}}{\hbar}E_n^+T} - e^{-\frac{\mathrm{i}}{\hbar}E_n^-T}. \tag{B.5}$$

We then obtain

$$\frac{\mathrm{Tr}(\hat{S}\hat{\Pi}_n\hat{U})}{\mathrm{Tr}(\hat{\Pi}_n\hat{U})} = \mathrm{i}\tan(\frac{\Delta E_n}{2\hbar}T). \tag{B.6}$$

where $\Delta E_n = E_n^- - E_n^+$. If the condition

$$\frac{|T|\Delta E_n}{2\hbar} \ll 1 \tag{B.7}$$

is satisfied, the tunnelling splitting ΔE_n can be explicitly written as

$$\Delta E_n \sim \frac{2\hbar}{\mathrm{i}T}\frac{\mathrm{Tr}(\hat{S}\hat{\Pi}_n\hat{U})}{\mathrm{Tr}(\hat{\Pi}_n\hat{U})}. \tag{B.8}$$

We now rewrite the right-hand side of (B.8) in the path integral form. Introducing the quasi-mode $|\Phi_n\rangle = (|\phi_n^+\rangle + |\phi_n^-\rangle)/\sqrt{2}$, the projection operator is expressed as

$$|\phi_n^+\rangle\langle\phi_n^+| + |\phi_n^-\rangle\langle\phi_n^-| = |\Phi_n\rangle\langle\Phi_n| + \hat{S}|\Phi_n\rangle\langle\Phi_n|\hat{S}. \tag{B.9}$$

Let $\Phi_n^{sc}(q)$ be WKB approximation of $\Phi_n(q)$ [69, 70], which is localized on the energy curve satisfying $E \sim E^{\pm}$, then the numerator and denominator of the formula (B.8) are semiclassically evaluated as

$$2\int dqdq'\Phi_n^{sc}(q)(\Phi_n^{sc}(q'))^* G(\eta q', q; T), \tag{B.10}$$

where $G(\eta q', q; T)$ represents the Van Vleck-Gutzwiller propagator

$$G(\eta q', q; T) = \sum_\gamma (-1)^{k_\gamma}\sqrt{\det\left(\frac{\mathrm{i}}{2\pi\hbar}\frac{\partial^2 S_\gamma}{\partial q_f \partial q_i}\right)}e^{\frac{\mathrm{i}}{\hbar}S_\gamma(\eta q', q; T)}. \tag{B.11}$$

Here $\eta = -1$ for the numerator and $\eta = +1$ for the denominator of the formula (B.8), respectively. The index k_γ denotes the number of conjugation points along the trajectory γ.

We further evaluate the integral (B.10) again using the saddle point approximation, which requires the condition

$$\lim_{q_f \to \eta q_i} \frac{\delta S_\gamma}{\delta q_i} = \frac{\partial S_\gamma}{\partial q_i} + \frac{\partial q_f}{\partial q_i}\frac{\partial S_\gamma}{\partial q_f} = 0. \tag{B.12}$$

Then the generating relations

$$\frac{\partial S_\gamma}{\partial q_i} = -p_i, \qquad \frac{\partial S_\gamma}{\partial q_f} = \eta p_f, \tag{B.13}$$

leads to the condition

$$p_f = \eta p_i \tag{B.14}$$

for each η. By taking the trace of integral (B.10), the classical paths contributing to the final semiclassical sum should altogether satisfy the conditions $E \sim E_n^{\pm}$, $q_f = \eta q_i$ and $p_f = \eta p_i$. In section 3.1, q_f and q_i are expressed as $q(T)$ and $q(0)$, respectively (same as for p). After calculating the prefactor in evaluating the integral (B.10) (see details in Ref. [35]), we finally reach the formula (3.3).

Appendix C

Integral along γ loops

In this appendix we calculate the integral whose integration contour encircles a single branch point q_i of the function $p(q)$. In the text, such a loop is called the γ_i loop.

Branch points of the algebraic function are algebraic singularities, around which p has the Puiseux expansion in the following form

$$p(q) = \sum_{n=s}^{\infty} c_n (q - q_i)^{\frac{n}{w}}, \qquad (s > -\infty) \tag{C.1}$$

where w is a positive number.

Putting $t = (q - q_i)^{1/w}$, we evaluate each term of the expansion as

$$\frac{1}{2\pi \mathrm{i}} \int_C (q - q_i)^{\frac{n}{w}} dq = \frac{w}{2\pi \mathrm{i}} \oint t^{n+w-1} dt = \begin{cases} w & \text{if } n + w = 0 \\ 0 & \text{otherwise,} \end{cases} \tag{C.2}$$

where C is a closed curve circling around the point $q = q_i$ w times [71].

For a Hamiltonian of the form $H = p^2/2 + V(q)$ where $V(q)$ is a polynomial function of q, the function $p(q)$ does not contain negative order terms in the corresponding Puiseux series. Therefore the action integrals for the γ_i loops all vanish. For the normal form Hamiltonian (4.28), if the condition $2k > m$ holds, the γ_i contributions are all zero as well since the function $p(q)$ does not contain negative order terms in the Puiseux series. On the other hand, for $2k \leq m$, the coefficient for the highest order of p contains the variable q, resulting in a non-zero contribution from γ_i loops.

Appendix D

The action relation and the residue at infinity

In this appendix, we provide an explicit derivation of action relations. The following calculations can easily be generalised to the multi-well potential systems. We here present double- and triple-well cases as examples.

D.1 Double-well case

Let us consider the Hamiltonian:

$$H = \frac{p^2}{2} + V(q), \tag{D.1}$$

where $V(q) = E + (q - q_1)(q - q_2)(q - q_3)(q - q_4)$. Branch points of $p(q)$ at the energy E are located at $q = q_i$ $(1 \leq i \leq 4)$. Let C be a closed curve rotating clockwise around all branch points (figure D.1). The loop C is homotopic to the loop around infinity on the Riemann sphere, so the integration along this loop is equal to the residue of infinity. We calculate the residue at $q = +\infty$

as follows. Introducing a new coordinate $q = 1/\eta$, we find

$$\begin{aligned}\oint_{\Gamma^{(\infty)}} p(q)dq &= \oint \frac{1}{\eta^2}\sqrt{-W(\eta)}(\frac{-1}{\eta^2})d\eta \\ &= \oint \frac{-1}{\eta^4}\left(\sum_k C_k\eta^k\right)d\eta,\end{aligned}$$

where $W(\eta) := 2(1-q_1\eta)(1-q_2\eta)(1-q_3\eta)(1-q_4\eta)$, and C_k $(k \geq 0)$ are coefficients of the Taylor expansion of $\sqrt{-W(\eta)}$. $\Gamma^{(\infty)}$ denotes a single loop encircling $\eta = 0$. For the integration over η, the loop rotates anticlockwise around $\eta = 0$, and the residue is evaluated as $-2\pi\mathrm{i}C_3$. An explicit form of C_3 is

$$\begin{aligned}C_3 &= \mathrm{i}\Big(\frac{1}{4}(q_1+q_2+q_3+q_4)(q_1q_2+q_1q_3+q_2q_3-\frac{1}{4}(q_1+q_2+q_3+q_4)^2 \\ &\quad +q_1q_4+q_2q_4+q_3q_4)+\frac{1}{2}(-q_1q_2q_3-q_1q_2q_4-q_1q_3q_4-q_2q_3q_4)\Big).\end{aligned}$$

Hence we obtain $S^{(\infty)} := \oint_{\Gamma^{(\infty)}} p(q)dq = -2\pi\mathrm{i}C_3$.

On the other hand, we evaluate the same integral by taking the integration along the real axis. We introduce new coordinates r_{q_i} and θ_{q_i} as $r_{q_i}e^{\mathrm{i}\theta_{q_i}} := q - q_i$ $(1 \leq i \leq 4)$. Here we have to take a close look at the phase of the function $p(q)$ and the upper limit of the integration. If we take the phase as $p(q) = \mathrm{i}\sqrt{r_{q_1}r_{q_2}r_{q_3}r_{q_4}}$, the upper limit should satisfy the condition $q_4 < q$ in order that the phase of $p(q)$ is consistent with the residue calculation at infinity, as shown in figure D.1. We therefore obtain

$$\begin{aligned}\oint_C p(q)dq &= 2\int_{q_1}^{q_2} pdq - 2\int_{q_3}^{q_4} pdq \\ &= S_L - S_R.\end{aligned} \tag{D.2}$$

Finally we get the relation (4.8)

$$S^{(\infty)} = \oint_{\Gamma^{(\infty)}} p(q)dq = \oint_C p(q)dq = S_L - S_R. \tag{D.3}$$

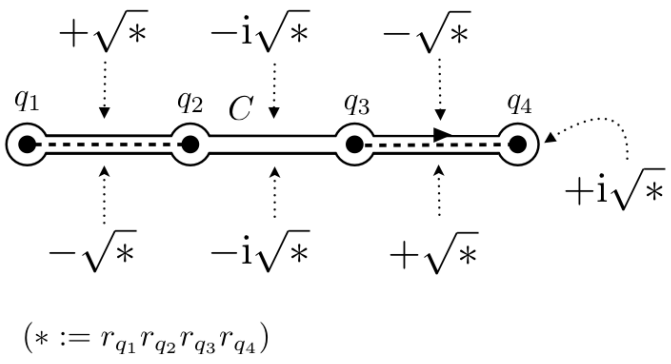

Figure D.1: The integration contour C and the phase of $p(q)$ at each position. The black dots are branch points. The dash lines represent the branch cuts.

D.2 Triple-well case

For the triple-well case where $V(q) = E + (q-q_1)(q-q_2)(q-q_3)(q-q_4)(q-q_5)(q-q_6)$, we find

$$\begin{aligned} \oint_{\Gamma^{(\infty)}} p(q)dq &= \oint \frac{1}{\eta^3}\sqrt{-W(\eta)}(\frac{-1}{\eta^2})d\eta \\ &= \oint \frac{-1}{\eta^5}\left(\sum_k C_k \eta^k\right) d\eta. \end{aligned}$$

Here $W(\eta) := 2(1-\eta q_1)(1-\eta q_2)(1-\eta q_3)(1-\eta q_4)(1-\eta q_5)(1-\eta q_6)$, and C_k $(k \geq 0)$ are coefficients of the Taylor expansion of $\sqrt{-W(\eta)}$. The residue is evaluated as $-2\pi\mathrm{i}C_4$. Hence we obtain $S^{(\infty)} := \oint_{\Gamma^{(\infty)}} p(q)dq = -2\pi\mathrm{i}C_4$.

On the other hand, we calculate the same integral along the real axis. As shown in figure D.2, we choose a closed curve C rotating clockwise around all branch points, and introduce new coordinates r_{q_i} and θ_{q_i} as $r_{q_i}e^{\mathrm{i}\theta_{q_i}} := q - q_i$ $(1 \leq i \leq 6)$. If we take the phase as $p(q) = \mathrm{i}\sqrt{r_{q_1}r_{q_2}r_{q_3}r_{q_4}r_{q_5}r_{q_6}}$, the upper limit should satisfy the condition $q_6 < q$ in order that the phase of $p(q)$ should be consistent with the residue calculation at infinity, as shown in figure D.2.

Then we obtain

$$\begin{aligned} \oint_C p(q)dq &= -2\int_{q_1}^{q_2} pdq + 2\int_{q_3}^{q_4} pdq - 2\int_{q_5}^{q_6} pdq \\ &= -S_L + S_C - S_R. \end{aligned} \tag{D.4}$$

Finally we reach the relation (4.21)

$$S^{(\infty)} = -S_L + S_C - S_R. \tag{D.5}$$

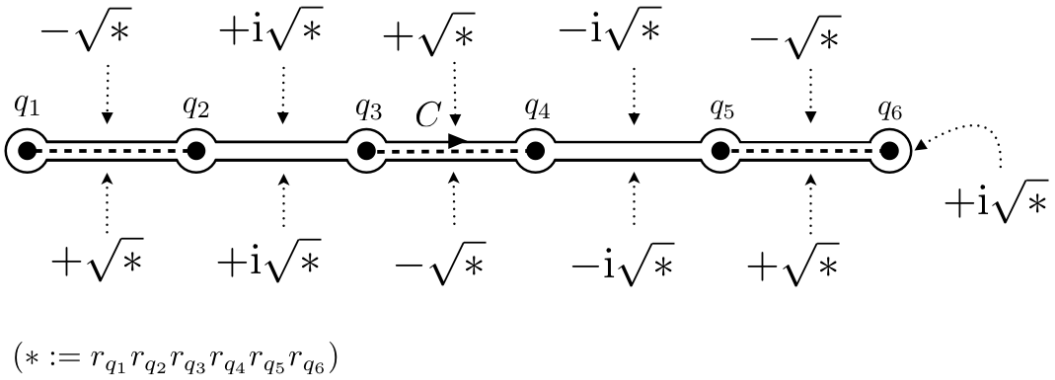

Figure D.2: The integration contour C and the phase of $p(q)$ at each position. The black dots are branch points. The dash lines represent the branch cuts.

Acknowledgments

I would like to express my deepest appreciation to Akira Shudo of his stimulating and patient supervision of this thesis. I am truly grateful for his cordial supports, advices and all aspects of his helping during the course of Ph.D student. I also would like to thank Takashi Hotta and Hiroyuki Mori for careful reading of this thesis. I would like to thank Amaury Mouchet and Jérémy Le Deunff for fruitful discussions and advices on formulation of tunnelling splitting and complex classical dynamics. I am very grateful to Masanori Kobayashi for many valuable comments on the fundamental group for algebraic functions. I would like to thank Kensuke S. Ikeda and Kin'ya Takahashi for stimulating discussions and advices on quantum tunnelling and complex analysis. I am grateful to Masafumi Yoshino for careful reading and stimulating discussions on Appendix A.2 and A.3. I would like to thank Roland Ketzmerick, Denis Ullmo, Steven Tomsovic, Oliver Brodier, Peter Schlagheck and Arnd Bäcker for stimulating discussions at the conference "Quantum chaos: fundamentals and applications". I would like to thank the members of the Nonlinear Physics Group, Yasutaka Hanada, Normann Mertig, Kensuke Yoshida, Hajime Yoshino, Naoaki Shimada, Chihiro Tsubota and Kota Kanno for stimulating discussions and their encouragement. Especially, I would like to thank Atsushi Tanaka for maintaining the computational environment, discussions on quantum tunnelling, and his cordial encouragement. I also would like to thank the former members of our group, especially Akira Akaishi, Yasuyuki Hodoshima and Ikumi Maeda for their encouragement. I would like to thank Satoru Saito, Takahumi Shimizu, Tukasa Yumibayashi and Yuki Wakimoto for their genial encouragement. Finally, I special thanks to my family for continuing supports and understanding.

Bibliography

[1] W. A. Lin and L. E. Ballentine, Phys. Rev. Lett., **65**, 2927, (1990)

[2] O. Bohigas, S. Tomsovic and D. Ullmo, Phys. Rev. Lett., **64** 1479 (1990)

[3] O. Bohigas, S. Tomsovic and D. Ullmo, Phys. Rep., **223** 43 (1993)

[4] R. Roncaglia, L. Bonci, F. M. Izrailev, B. J. West and P. Grigolini, Phys. Rev. Lett., **73** 802 (1994)

[5] S. Tomsovic and D. Ullmo, Phys. Rev. E, **50** 145 (1994)

[6] O. Brodier, P. Schlagheck and D. Ullmo, Phys. Rev. Lett., **87** 064101 (2001)

[7] O. Brodier, P. Schlagheck and D. Ullmo, Ann. Phys., **300** 88 (2002)

[8] A. J. Lichtenberg and M. A. Lieberman, *Regular and Chaotic Dynamics*, Applied Mathematical Sciences (Springer New York) 2-nd revised edition (1992)

[9] L. E. Reichl, *The Transition to Chaos: Conservative Classical Systems and Quantum Manifestations*, (Springer New York) 2-nd edition (2012)

[10] V. I. Arnold, *Mathematical Methods of Classical Mechanics*, New York/Berlin: Springer-Verlag, (1978)

[11] M. J. Davis and E. J. Heller, J. Chem. Phys., **75** 246 (1981)

[12] S. Keshavamurthy and P. Schlagheck, *Dynamical Tunnelling: Theory and Experiment*, CRC Press (2011)

[13] S. C. Creagh, in *Tunnelling in complex systems* edited by S. Tomsovic (World Scientific, Singapore) p. 35 (1988)

[14] L. D. Landau and E. M. Lifshitz, *Quantum Mechanics (Non-relativistic Theory), Course of Theoretical Physics*, 3rd ed. (Oxford: Pergamon Press) Vol 3 (1977)

[15] J. N. L. Connor, T. Uzer, R. A. Marcus and A. D. Smith, J. Chem. Phys., **80** 5095 (1984)

[16] A. Garg, Amer. J. Phys., **68** 430 (2000)

[17] K. T. Hecht, *Quantum Mechanics*, New York: Springer-Verlag (2000)

[18] B. Sakita and K. Kitsukawa, *Keirosekibun niyoru tajiyudo no ryoshirikigaku*, Iwanamishoten (1986) (in Japanese)

[19] L. S. Schulman, *Techniques and Applications of Path Integration*, J. Wiley & Sons, inc., New York (1981)

[20] J. S. Langer, Ann. Phys., **54** 258 (1969)

[21] S. Coleman, *Aspects of Symmetry (selected Erice lectures)*, Cambridge: Cambridge University Press (1985)

[22] S. C. Creagh and N. D. Whelan, Ann. Phys. (N. Y.), **272** 196 (1999)

[23] K. F. Freed, J. Chem. Phys., **56** 692 (1972)

[24] T. F. George and W. H. Miller, J. Chem. Phys., **56** 5722 (1972)

[25] W. H. Miller, Adv. Chem. Phys., **25** 69 (1974)

[26] U. Weiss and W. Haeffner, Phys. Rev. D, **27** 2916 (1983)

[27] R. D. Carlitz and D. A. Nicole, Ann. Phys. (N. Y.), **164** 411 (1985)

[28] E. M. Ilgenfritz and H. Perlt, J. Phys. A, **25** 5729 (1992)

[29] A. Shudo and K. Ikeda, Physica D, **115**, 234-292 (1997)

[30] A. Shudo, Y. Ishii and K.S. Ikeda, J. Phys. A: Math. Theor., **42** 265101 (2008); J. Phys. A: Math. Theor., **42** 265102 (2009)

[31] K. Takahashi and K. S. Ikeda, Ann. Phys., **283** 94 (2000)

[32] K. Takahashi and K. S. Ikeda, Foundations of Physics, **31** 177 (2001)

[33] K. Takahashi, A. Yoshimoto and K. S. Ikeda, Physics Letters A, **297** 370 (2002)

[34] A. Shudo and K.S. Ikeda, in *Dynamical Tunnelling* edited by Srihari Keshavamurthy and Peter Schlagheck (CRC Press) Chapter 7, p.139 (2011)

[35] J. Le Deunff and A. Mouchet, Phys. Rev. E, **81** 046205 (2010)

[36] P. Schlagheck, A. Mouchet and D. Ullmo, *Dynamical Tunnelling:Theory and Experimental* (CRC Press) Chap. 8 (2011)

[37] B. V. Chirikov, *Research concerning the theory of nonlinear resonance and stochasticity*, Institute of Nuclear Physics, Novosibirsk (1969)

[38] A. Mouchet, J. Phys. A, **40**, F663 (2007)

[39] L. Bonci, A. Farusi, P. Grigolini and R. Roncaglia, Phys. Rev. E **58** 5689 (1998)

[40] S. Löck, A. Bäcker, R. Ketzmerick and P. Schlagheck, Phys. Rev. Lett. **104** 114101 (2010)

[41] Y. Hanada, A. Shudo and K. S. Ikeda, Phys. Rev. E, **91**, 042913 (2015)

[42] Y. Hanada, A. Shudo and K. S. Ikeda, *Special Issue of Advances in Science, Technology and Environmentology* (Waseda University), **B11**, 127-130 (2015)

[43] J. Le Deunff, A. Mouchet and P. Schlagheck, Phys. Rev. E, **88** 042927 (2013)

[44] G. D. Birkhoff, *Dynamical Systems*, New York: American Mathematical Society Colloquium Publications Vol IX (1927)

[45] F. G. Gustavson, Astronomical Journal, **71** 670 (1966)

[46] H. Weyl, *The Theory of Group and Quantum Mechanics*, Dover Publications, New York (1950)

[47] J. R. Shewell, American Journal of Physics, **27** 16 (1956)

[48] H. -J. Stöckmann, *Quantum Chaos : an introduction*, Cambridge university press (1999)

[49] V. P. Maslov and M. V. Fedoriuk, *Semi-Classical Approximation in Quantum Mechanics*, Boston: Reidel (1981)

[50] A. Voros, Ann. Inst. H. Poincare A, **39** 211 (1983)

[51] E. Delabaere, H. Dillinger and F. Pham, J. Math. Phys., **37** 6126 (1997)

[52] T. Kawai and Y. Takei, *Algebraic Analysis of Singular Perturbation Theory*, Translations of Mathematical Monographs, AMS (2006)

[53] N. Honda, T. Kawai and Y. Takei, *Virtual Turning Points* SpringerBriefs in Mathematical Physics (2015)

[54] M. Tsuji, *Kansuron gekan*, Asakurashoten (1952) (in Japanese)

[55] W. Schlag, *A Course in Complex Analysis and Riemann Surfaces, Graduate Studies in Mathematics*, Providence Rhode Island: American Mathematical Society Vol. 154 (2014)

[56] C. Kosniowski, *A First Course in Algebraic Topology*, Cambridge: Cambridge University Press (1980)

[57] D. Bohm, *Quantum Theory*, Prentice Hall, Englewood Cliffs, N. J. (1951)

[58] D. Khuat-duy and P. Leboeuf, Appl. Phys. Lett., **63** 1903 (1993)

[59] H. M. Farkas and I. Kra, *Riemann Surfaces*, New York/Berlin: Springer-Verlag (1980)

[60] A. Shudo and K.S. Ikeda, Nonlinearity, **29** 375 (2016)

[61] T. Gulden, M. Janas, P. Koroteev and A. Kamenev, Journal of Experimental and Theoretical Physics, **117** 3 517-537 (2013)

[62] T. Gulden, M. Janas and A. Kamenev, J. Phys. A, **48** 075304 (2015)

[63] M. Toda, *Daenkansu nyumon*, Nipponhyoronsha (1976) (in Japanese)

[64] A. Hurwitz and R. Courant, *Daenkansuron*, translated by N. Adachi and K. komatsu, Springer-Verlag Tokyo, Inc (1991) (in Japanese)

[65] S. Tomochika, *Daenkansuron*, Gendaikogakusya (1942) (in Japanese)

[66] K. R. Meyer, Trans. Amer. Math. Soc., **149** 95 (1970)

[67] P. Leboeuf and A. Mouchet, Ann. Phys., **275** 54 (1999)

[68] A. M. Ozorio de Almeida and J. H. Hannay, J. Phys. A, **20** 5873 (1987)

[69] J. B. Keller, Ann. Phys. (N. Y.), **4** 180 (1958)

[70] I. C. Percival, Adv. Chem. Phys., **36** 1 (1977)

[71] T. Ishizu and O. Saito, *Kansuron to sono ouyo (The theory of Functions and the Applications)*, Coronasya (1958) (in Japanese)